Kaunas University of Technology

Faculty of Electrical and Electronics Engineering

A Comparative Study of Methods for Unobtrusive Long-Term Monitoring of Blood Pressure Parameters

Master's Final Degree Project

Keerthik Dhivya Rajakumar

Project author

Prof. dr. Vaidotas Marozas

Supervisor

Asst. Birute Paliakaite

Co-Supervisor

Kaunas, 2019

Kaunas University of Technology

Faculty of Electrical and Electronics Engineering

A Comparative Study of Methods for Unobtrusive Long-Term Monitoring of Blood Pressure Parameters

Master's Final Degree Project

Biomedical Engineering (6211EX002)

Keerthik Dhivya Rajakumar

Project author

Prof. dr. Vaidotas Marozas

Supervisor

Prof. dr. Linas Svilainis

Reviewer

Kaunas, 2019

Kaunas University of Technology

Faculty of Electrical and Electronics Engineering

Keerthik Dhivya Rajakumar

A Comparative Study of Methods for Unobtrusive Long-Term Monitoring of Blood Pressure Parameters

Declaration of Academic Integrity

I confirm that the final project of mine, Keerthik Dhivya Rajakumar, on the topic "A Comparative Study of Methods for Unobtrusive Long-Term Monitoring of Blood Pressure Parameters" is written completely by myself; all the provided data and research results are correct and have been obtained honestly. None of the parts of this thesis have been plagiarised from any printed, Internet-based or otherwise recorded sources. All direct and indirect quotations from external resources are indicated in the list of references. No monetary funds (unless required by Law) have been paid to anyone for any contribution to this project.

I fully and completely understand that any discovery of any manifestations/case/facts of dishonesty inevitably results in me incurring a penalty according to the procedure(s) effective at Kaunas University of Technology.

(name and surname filled in by hand)	(signature)

Rajakumar Keerthik Dhivya. A Comparative Study of Methods for Unobtrusive Long-Term Monitoring of Blood Pressure Parameters. Master's Final Degree Project / supervisor prof. Vaidotas Marozas; Faculty of Electrical and Electronics Engineering, Kaunas University of Technology.

Study field and area (study field group): Bioengineering, Engineering Sciences.

Keywords: electrocardiogram, photoplethysmogram, pulse arrival time, middle amplitude, slope sum function, matched filter, estimation model.

Kaunas, 2019. 49 pages.

Summary

Nocturnal non-dipping and morning surge in blood pressure for hypertensive patients are strong risk factors for cardiovascular events if untreated for prolonged time. Even though means for continuous and non-continuous monitoring of blood pressure parameters are available, there is a lack of methods for unobtrusive long-term monitoring. In this thesis, three different methods of pulse arrival time estimation from synchronously recorded electrocardiogram and photoplethysmogram are compared and later correlated with blood pressure parameters, such as systolic blood pressure, diastolic blood pressure, mean blood pressure and pulse pressure. The selected methods are middle amplitude of pulse slope, peaks of slope sum function and peaks of matched filtered photoplethysmogram. These methods are tested on thermal stress test database and breathing test database. The results were tested with two models such as Moens-Korteweg exponential arterial elasticity model and derivative of Moens-Korteweg linear model. The results show that volunteers from breathing test database have higher correlation than thermal stress test database. Also, the volunteers from breathing test database have moderate (0.4–0.59) to strong (0.6–0.79) downhill correlation for systolic blood pressure, mean blood pressure and pulse pressure, and very weak (0.0–0.19) to weak (0.2–0.39) correlation for diastolic blood pressure especially for middle amplitude of pulse slope method. When blood pressure estimation models based on pulse arrival time were created and tested, the correlation of real and predicted systolic blood pressure is moderate (0.4–0.59) to strong (0.6–0.79). Moreover, the models have good response such that their mean difference is <5 mmHg and standard deviation of difference is <8 mmHg when tested on systolic blood pressure and the results are similar for all three evaluated methods.

Rajakumar Keerthik Dhivya. Kasdienės veiklos nevaržančių ilgalaikės kraujospūdžio parametrų stebėsenos metodų palyginimas. Magistro baigiamasis projektas / vadovas prof. Vaidotas Marozas; Kauno technologijos universitetas, Elektros ir elektronikos fakultetas.

Studijų kryptis ir sritis (studijų krypčių grupė): Bioinžinerija, inžinerijos mokslai.

Reikšminiai žodžiai: elektrokardiograma, fotopletizmograma, pulsinės bangos atvykimo laikas, pusinė amplitudė, suminė fronto funkcija, suderintas filtras, įvertinimo modelis.

Kaunas, 2019. 49 p.

Santrauka

Naktinio kraujospūdžio sumažėjimo nebuvimas ar staigus rytinis kraujospūdžio padidėjimas yra svarbūs širdies ir kraujagyslių ligų ūminių įvykių veiksniai hipertenzija sergantiems pacientams. Nors nuolatinio ar protarpinio kraujospūdžio stebėjimo metodai yra prieinami, tačiau vis dar trūksta kasdienės veiklos nevaržančių ilgalaikės kraujospūdžio stebėsenos metodų. Šiame darbe lyginami trys pulsinės bangos atvykimo laiko vertinimo iš sinchroniškai užregistruotos elektrokardiogramos ir fotopletizmogramos metodai. Įvertinama šiais metodais gautų pulsinės bangos atvykimo laiko verčių koreliacija su kraujo spaudimo parametrais, tokiais kaip sistolinis, diastolinis, vidutinis ir pulsinis kraujo spaudimas. Charakteringam pulsinės bangos atvykimo taškui rasti naudoti metodai: pusinė pulso fronto amplitudė, suminės fronto funkcijos maksimumas ir suderintuoju filtru nufiltruotos fotopletizmogramos maksimumas. Šiems metodams ištestuoti naudotos šiluminio streso ir kvėpavimo testo duomenų bazės. Kraujospūdžio parametrams įvertinti panaudoti du modeliai: Moens-Korteweg eksponentinis arterinio elastingumo modelis ir išvestinis Moens-Korteweg tiesinis modelis. Tyrimo rezultatai rodo, kad analizuojant kvėpavimo testo duomenų bazę gaunama didesnė pulsinės bangos atvykimo laiko ir kraujo spaudimo parametrų koreliacija nei analizuojant šiluminio streso duomenų bazę. Kvėpavimo testo duomenų bazėje gaunama vidutinė (0.4–0.59) arba stipri (0.6–0.79) neigiama koreliacija sistoliniam, vidutiniam ir pulsiniam kraujo spaudimui, ir silpna arba labai silpna koreliacija diastoliniam kraujo spaudimui, ypač taikant pusinės pulso fronto amplitudės metodą. Sudarius kraujo spaudimo vertinimo iš pulsinės bangos atvykimo laiko modelius, gauta vidutinė (0.4–0.59) arba stipri (0.6–0.79) koreliacija tarp realių ir modeliu prognozuojamų sistolinio kraujo spaudimo verčių. Be to, abu modeliai pademonstravo gerą sutapimą, kadangi vidutinis skirtumas tarp realių ir prognozuojamų sistolinio kraujo spaudimo verčių buvo mažesnis nei 5 mmHg, o skirtumo standartinis nuokrypis nesiekė 8 mmHg visiems trims tirtiems metodams.

Acknowledgement

I would like to thank my supervisor Dr. Vaidotas Marozas and co-supervisor Birutė Paliakaitė for supporting me throughout this thesis with their valuable comments and ideas.

I express my special thanks and gratefulness to Birutė Paliakaitė who has spent enough time for me, guided me and provided immense support during the experiment that is used in this thesis and the implementation of the ideas. I am also thankful to Dr. Andrius Rapalis who guided through the handling of experiment's devices and collection of the signals. Finally, I thank all the volunteers of experiment who provided their presence despite of their work.

Table of contents

List of abbreviations and terms

Abbreviations:

BP – blood pressure;

CO – cardiac output;

CVS – cardiovascular system;

CVD – cardiovascular disease;

DBP – diastolic blood pressure;

ECG – electrocardiogram;

MBP – mean blood pressure;

PAT – pulse arrival time;

PP – pulse pressure;

PPG – photoplethysmogram;

PTT – pulse transit time;

PWV – pulse wave velocity;

SBP – systolic blood pressure;

SSF – slope sum function;

SVR – systemic vascular resistance;

MK – Moens-Korteweg and exponential arterial elasticity model;

L-DMK – derivative of Moens-Korteweg and linear model;

Introduction

One of the major fatal diseases globally is cardiovascular disease (CVD), and hypertension is the foremost risk factor for many CVD diseases such as arterial stiffness [1], aortic wall calcification, arrhythmia [2], ventricular ectopic beats [3][4], chronic kidney dysfunction, heart failure, aortic and peripheral artery malfunctions [5]. Early detection of these diseases can save lives and it has become a vital health challenge all over the world. Hypertensive patients with non-dipping nocturnal blood pressure (BP) and morning surge in BP are at higher risk of CVD like stroke, left ventricular hypertrophy, myocardial ischemia, increase in QTc dispersion and duration, decrease in left ventricular diastolic function, thickening of intima-media of vessels, arterial stiffness and susceptible plaques [5]–[8]. Hence BP is an early indicator to be diagnosed and monitored in long term. It can be measured either invasively or non-invasively by using different types of devices and techniques [9]. Although invasive methods can provide continuous monitoring of BP, it has some limitations such as the risk of infection, bleeding, hematoma, arterial thrombosis and even nerve damage. Therefore, in recent years, non-invasive BP measuring methods have received considerable research attention. Non-invasive monitoring of BP is classified into continuous and non-continuous monitoring. Non-continuous BP monitoring includes Riva-Rocci technique, mercury sphygmomanometer, auscultatory method and oscillometric method; whereas continuous BP monitoring methods are Penaz technique, arterial tonometry, pulse transit time (PTT) estimation, photometric method [9] and pulse arrival time (PAT). Since all non-invasive continuous BP monitoring methods except PTT and PAT requires inflation of a cuff, this thesis concentrates on PAT method for long term BP monitoring [10]. BP is conventionally characterized by four parameters: systolic blood pressure (SBP), diastolic blood pressure (DBP), mean blood pressure (MBP) and pulse pressure (PP). Photoplethysmography (PPG) is a device that calculates the changes in blood volume by utilizing a light source and a photo detector. As the skin is illuminated by the light from the light source, the light is absorbed by the blood in the arteries and the intensity of the reflected light changes which is measured by the photo detector.

By using PPG and electrocardiogram (ECG) signals, it is possible to measure BP in long-term with the help of PAT method. PAT is the time period between the R peaks of the ECG and peaks or other fiducial points of the PPG slope. This thesis elaborately defines three different methods to calculate PAT using thermal stress test database and breathing test database and provides the comparative results of these methods. These methods are different in terms of PPG peak detection and they are: slope sum function (SSF) [11][12], middle amplitude of pulse slope [13] and matched filtering [14]. Later PAT values are estimated for these methods and the three different PAT values obtained are checked for correlation with SBP, DBP, MBP and PP. Moens-Korteweg exponential arterial elasticity model and derivative of Moens-Korteweg linear model were created and tested on SBP to find their response for all PAT methods.

The aim of this thesis is to investigate methods based on pulse arrival time estimation for long-term monitoring of blood pressure parameters unobtrusively.

The objectives of this thesis are the following:

1. To perform a scientific literature review concerning blood pressure monitoring.
2. To implement the selected algorithms for pulse arrival time estimation.
3. To test the implemented algorithms on the collected signal database.

4. To perform a comparative study of the selected models for estimation of blood pressure parameters.

1. An overview of cardiovascular background and physiological signals

This chapter consists of the physiological background of cardiovascular system in section 1.1, blood pressure and blood pressure parameters (see section 1.2), consequences of nocturnal BP and morning surge in BP on cardiovascular disease patients (see section 1.3) and photoplethysmography and electrocardiography signal's pathophysiological overview and their acquisition (see section 1.4).

1.1. Anatomy of cardiovascular system

One of the important physiological systems in a human is cardiovascular system (CVS) which includes the main purposes [15]:

1. Transportation of oxygen, nutrients and water to all the tissues and organs of body and removal of unwanted products from the body.
2. Secretion and supplying of hormones.
3. Maintaining the body temperature.

The human circulatory system or CVS consists of two main circulatory loops namely, the pulmonary circulation and the systemic circulation. The heart is a part of circulatory system which is a muscular organ approximately in the size of a closed fist which has four chambers such as right and left auricle, right and left ventricle. The heart is liable for transporting oxygen, nutrients, hormones and waste products from the cells throughout the body. The wall of the heart is formed of three layers namely epicardium (the outermost layer), myocardium (middle layer that contains cardiac muscle tissue), endocardium (inner layer) [16]. The location of the human heart, lungs and kidneys along with their interconnection with blood transfusion is shown in Fig.1.1.

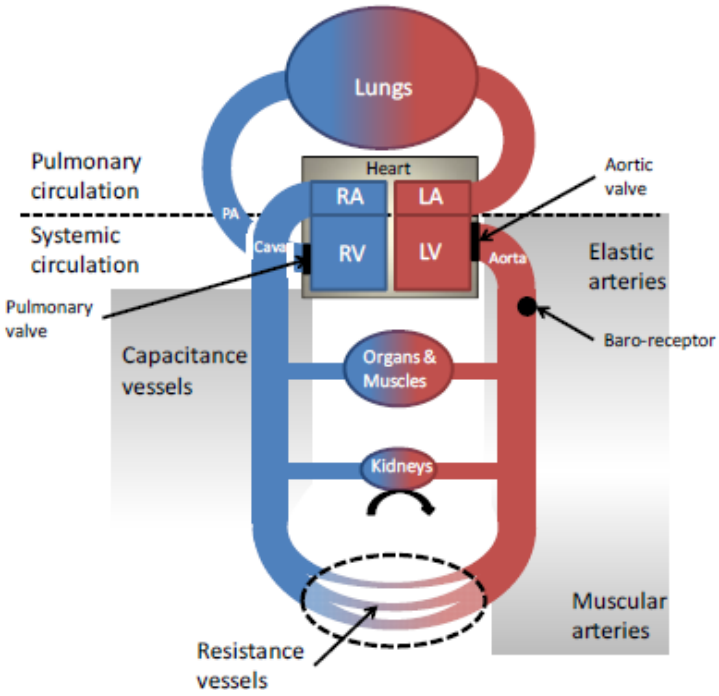

Fig.1.1. Cardiovascular system showing the pulmonary and systemic circulation, location of vital organs and their interconnection and blood pressure sensing baroreceptor, RA – right auricle, LA – left auricle, RV – right ventricle, LV – left ventricle, respectively, adapted from [15].

The heart can generate its own rhythm and the conduction is initiated by the pacemaker known as sinoatrial (SA) node, then passed to atrioventricular (AV) node through the AV bundle. The AV bundle later divides into left and right branches to touch the apex of the heart through Purkinje fibers that stimulates the cardiac muscle cells to contract.

The pulmonary circulation involves in the collection of deoxygenated blood from the heart to the lungs through the pulmonary artery and supplies oxygen to the blood in the lungs and go back to the heart again through pulmonary vein. The systemic circulation carries the oxygenated blood from the heart through the aorta and supplies the oxygenated blood to the whole body. Arteries carry these oxygenated bloods with maximum force pumped from the heart and hence they experience maximum BP. To sustain this force and pressure, arterial wall is thick, elastic and muscular enough so that as the pressure increases, the stretching of arterial wall also increases. Smaller arteries are provided with more muscular walls and hence they supply blood to small areas and maintains the regulation of blood flow. Arterioles are the end of the arterial branch which experience minimum BP since they are large numbered, reduced blood volume and far away from the direct pressure of the heart. Capillaries collect blood from arterioles and exchanges gases, nutrients and waste products between the tissues and blood using an endothelium filtrate. At the end of this process, the systemic circulation takes away the impurities from all tissues in the form of deoxygenated blood and reaches the heart for the next cycle of circulation.

1.2. Blood pressure and blood pressure parameters

As the blood is travelling throughout the blood vessels ranging from larger diameter in size to smaller one, the pressure exerted on the vessel wall is important which is known as BP. Regulation of BP is an important role of CVS in order to maintain the proper BP in vital organs like brain, heart or kidneys [15]. The information about BP and blood flow are sensed by baro-receptors and transmits it to the central nervous system (CNS). When the information about BP is passed through Autonomic Nervous System (ANS), the baroreflex changes the function of heart and blood vessels to attain focused BP values which in turn changes the cardiac output (CO) and systemic vascular resistance (SVR). CO is the amount of blood exerted from heart into aorta in l/min whereas SVR is resistance of fluid against the blood flow in mm Hg min/l. To maintain BP in long term, kidney controls the extra cellular fluid volume i.e. volume of fluids outside the all cells of the body. BP can be expressed as the product of CO and SVR i.e.

$$BP = CO \times \text{SVR} \qquad (1)$$

BP is represented in the form of four BP parameters such as SBP, DBP, MAP and PP based on one cardiac cycle. During systolic event of the cardiac cycle, the blood is driven out from the heart into the arteries by closing the tricuspid valve followed by aortic or pulmonary valve as a result of ventricular contraction [17]. The pressure that is exerted at the time of systolic event on blood vessels is known as SBP. As the next phase, during diastolic event, the blood is filled into heart once the aortic or pulmonary valve and tricuspid valve closes and it is said to be ventricular relaxation. The pressure that is exerted during diastolic event is known as DBP. The global normal pressure range of SBP/ DBP is 120/80 and it is represented in terms of mm/Hg units.

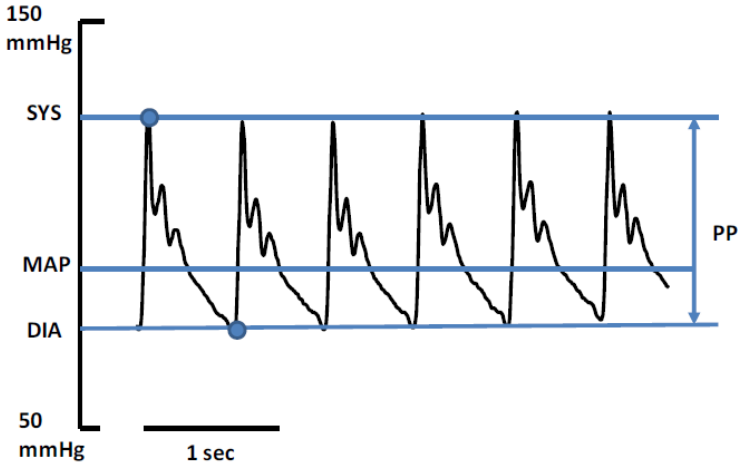

Fig.1.2. Arterial blood pressure waveform showing SBP as the peak or maximum of the pulse, DBP as the foot or minimum of the pulse, MAP and PP, adapted from [15].

The above Fig.1.2 shows six waveforms of arterial blood pressure of a human whose SBP, DBP, MBP and PP are marked in blue line. In other words, SBP and DBP are the maximum (peak) and minimum (foot) of an arterial blood pressure. MBP is the average of SBP and DBP but not defined by a simple averaging formula. MBP is expressed by two different formulas:

$$MBP = \frac{(SBP+2DBP)}{3} \tag{2}$$

$$MBP = DBP + \frac{PP}{3} \tag{3}$$

In equation 2, MBP is analysed as one third of SBP and DBP multiplied by two [15] whereas in equation 3, MBP is not the normal average of SBP and DBP because the ventricles spend longer time for DBP rather than SBP [18] . MBP is directly proportional to CO and it is the product of CO and total peripheral resistance.

$$MBP = CO \times Total\ Peripheral\ Resistance \tag{4}$$

The normal range of MBP is approximately between 75mmHg and 105mmHg [19]. PP is the common difference between SBP and DBP and so it ranges approximately 40mmHg.

$$PP = SBP - DBP \tag{5}$$

$$PP = \frac{Stroke\ Volume}{Arterial\ Compliance} \tag{6}$$

PP is directly proportional to stroke volume which is the volume of blood expelled from heart for every contraction in l minute and inversely proportional to arterial compliance that is as the compliance increases from capillaries to aorta, PP decreases [20].

1.3. Morning surge and nocturnal blood pressure in cardiovascular disease

The major risk factor of CVD is unhygienic diet, lack of exercises, intake of large amount of tobacco and alcohol. This relatively express in individuals as high BP, high blood glucose level, high blood lipids and obesity due to the deposition of fats on the inner wall of the blood vessels that causes

blockage in the blood vessels delivering the blood to the heart. According to WHO, CVD are a cluster of diseases of the heart and blood vessels which includes coronary heart disease, cerebrovascular disease, peripheral arterial disease, rheumatic heart disease, congenital heart disease and deep vein thrombosis and pulmonary embolism. If CVD is untreated for a prolonged time, it would lead to heart attack or atherosclerosis especially for those who with high risk factors such as hypertension, diabetes or hyperlipidaemia.

Henceforth, an early prediction of CVD is most essential to reduce the sudden death and it is straightforward to predict in hypertensive patients. In several studies it is evident that hypertensive patients with non-dipping nocturnal BP and morning surge in BP are at higher risk of CVD like stroke, left ventricular hypertrophy, myocardial ischemia, increase in QTc dispersion and duration, decrease in left ventricular diastolic function, thickening of intima-media of vessels, arterial stiffness and susceptible plaques [5], [6]. BP exhibits a diurnal variation by exhibiting a rapid incline in BP after waking up in morning is known as morning surge BP and decline of BP during night time is known as nocturnal BP. There are two events in nocturnal BP that is in hypertensive patients if the BP does not decline during night time, they are non-dippers while the others, whose BP decline during night time are dippers. Daily life activities shows a vital place in diurnal BP and it is proven that non-dippers have inclined BP during night time due to sleep disorder, obesity and high intake of sodium [21], and they are suspected to be at increased risk of CVD while alcohol ingestion and smoking would lead to inclination in morning BP. Non-dippers who are with or without morning surge greater than 23 mm Hg are at extreme risk of ischemic stroke compared to dippers while the SBP in dippers with inclined morning surge are at risk of ischemic stroke [8],[10]. When the BP increases for nocturnal non-dippers or for morning surge, chamber of left ventricle increases and causes left ventricular hypertrophy. The reduction in sympathetic baroreflex activity in young and elder individuals have shown inclination in morning surge BP and this condition happens when the large arterial wall stiffens, the arterial baroreceptors stretches less in the arteries [23]. This condition even increases stroke volume and results in rapid inclination of morning surge BP especially SBP. QT interval in ECG represents the ventricular depolarization. QTc dispersion is measured as difference between highest and lowest QT interval in all 12 leads of ECG [24] and it is proven that QTc dispersion was longer in non-dippers than dippers. It is also proved that non-dippers may be suspected to ventricular arrhythmia. Therefore, it is significant to monitor morning surge BP and nocturnal BP especially for hypertensive patients to avoid risk of CVD.

1.4. Photoplethysmography and electrocardiography

BP can be measured non-invasively for long-term and their techniques will be seen later in Chapter 2. One of the techniques for long-term monitoring of BP is PPG and ECG which together can provide PAT. PAT correlates with BP which helps to measure non-invasively. PPG is a cost effective, non-invasive photosensitive technique which determines the change in blood volume in the microvascular bed of tissue. There are pulsatile AC component and DC component in a PPG waveform. AC component whose fundamental frequency is usually 1 Hz, measures the change in blood volume of CVS while the DC component changes gradually due to respiration, vasodilator and vasoconstrictor waves, thermoregulation, width of tissue construction, complexion and mean blood volume accordingly by the superimposition of AC component [25][26].

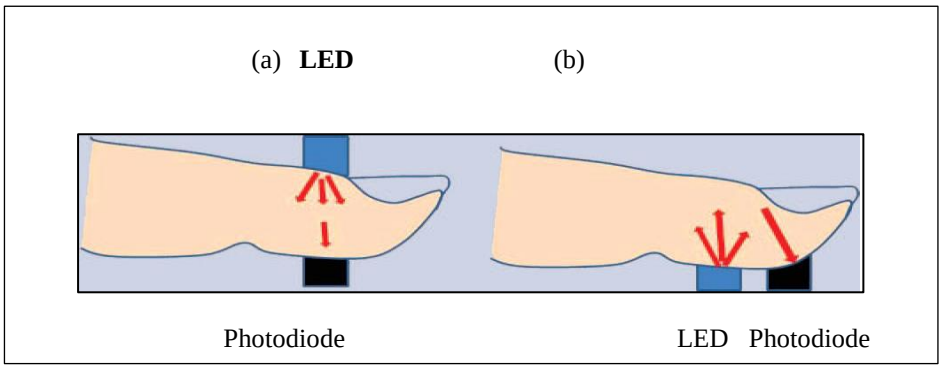

Fig.1.3. (a) PPG transmittance mode showing LED and photodiode placed in adjacent position, **(b)** PPG reflectance mode showing LED and photodiode placed in parallel position, adapted from [26].

PPG device which comprises of a probe with light source and a detector that detects arterial pulse wave which transmits through the body and this technique is non-contact with skin [27]. The light from the light source penetrates through the skin into the tissue and the reflected light is detected by a photodetector or a photodiode. The backscattered light provides the variations in blood volume related with every single heart-beat. In recent trend, the PPG sensors consists of light emitting diode (LED) as the light source and applicable photodetectors that works at the infrared wavelengths which may be either red or near infrared wavelengths or both and it senses in two ways as transmittance approach and reflectance approach as displayed in Fig. 1.3. The transmittance mode of PPG uses larger LED intensity while the reflectance uses comparatively low intensity. The bandwidth of LED is approximately 50 nm which switches into light energy from electrical energy. The photodetector which switches into electrical energy from light energy must be chosen based on the spectral features that match with the source of illumination.

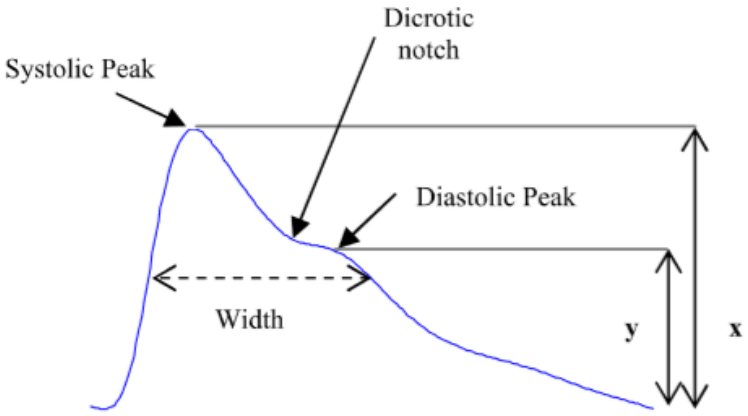

Fig.1.4. PPG waveform with amplitude of systolic peak (x) and diastolic peak (y), adapted from [27].

A single PPG waveform comprises of a systolic peak, diastolic peak and a dicrotic notch. The systolic peak represents the pressure wave that is travelling from the left ventricle of the heart to the fringe of the body whereas diastolic peak represents the pressure wave of arteries of the inferior body [28]. PPG can detect pulses from ear, finger or toe and it can be measured accurately by transmittance mode while the reflectance mode measures from any parts of the body. The penetration of light is inverse of absorption coefficient i.e. the higher the penetration, the lesser the absorption. Red and infrared light are commonly used in PPG sensors as they penetrates deeper into the tissue due to their low absorption coefficients from 650 nm to 850 nm [26]. When the LED and photodetector is kept in larger distance, the penetration will be higher. The normal distance among LED and photodetector

used is between 4 mm and 6 mm. The PPG signals of right- and left-hand fingertips do not have any evident for the difference in terms of heart rate variability when the study was conducted for 23 male healthy subjects and hence both hand's PPG signal can be utilized as a substitute [29].

The cardiac cell membranes are positively charged outside due to the presence of large number of cations outside called as resting membrane potential. In sodium-potassium pump mechanism, when sodium channels open, there is a rapid incoming of extracellular sodium or calcium ions through membrane into the cardiac cells followed by sudden closing of sodium channels to avoid further incoming of sodium ions and this process is called depolarization as the resting potential is inversed. Concurrently, when the potassium channels open, there is a rapid outgoing of intracellular potassium ions outside the cells along with active pumping out of sodium ions from the cardiac cells and this process regains the positivity of cells outside and it is called repolarization [30]. The electrocardiography (ECG) is the measure of electrical activity of the heart using skin electrodes. An ECG lead either connects the electrodes to the ECG machine or it is an assembly of electrodes. ECG wave is formed from three distinct activities [31]:

- Upward deflection is formed when electrical activity is towards a lead.
- Downward deflection is formed when electrical activity is away from a lead.
- Deflections of depolarization and repolarization appears in adjacent position.

The electrical activity is initiated by sinoatrial node of the heart. It produces the PQRST wave by reaction of electrical changes in the heart. For every cardiac cycle, a single PQRST wave is formed. The P wave is formed due to atrial depolarization with minimal deflection. QRS waves denotes ventricular depolarization while Q wave is former downward deflection formed due to septal depolarization and might be linked to breathing. R wave is the first upward deflection that represents major ventricular depolarization with largest deviation of wave whereas S wave represents the late ventricular depolarization. Finally, the T wave represents the repolarization of the ventricles and U wave represents papillary muscle repolarization. The distance in time between initial P wave deflection and initial QRS complex deflection is said to be PR interval while the distance in time between final QRS wave deflection and initial T wave reflection is called as ST segment or ST interval [31], [32]. ECG waveform is presented in Fig.1.5.

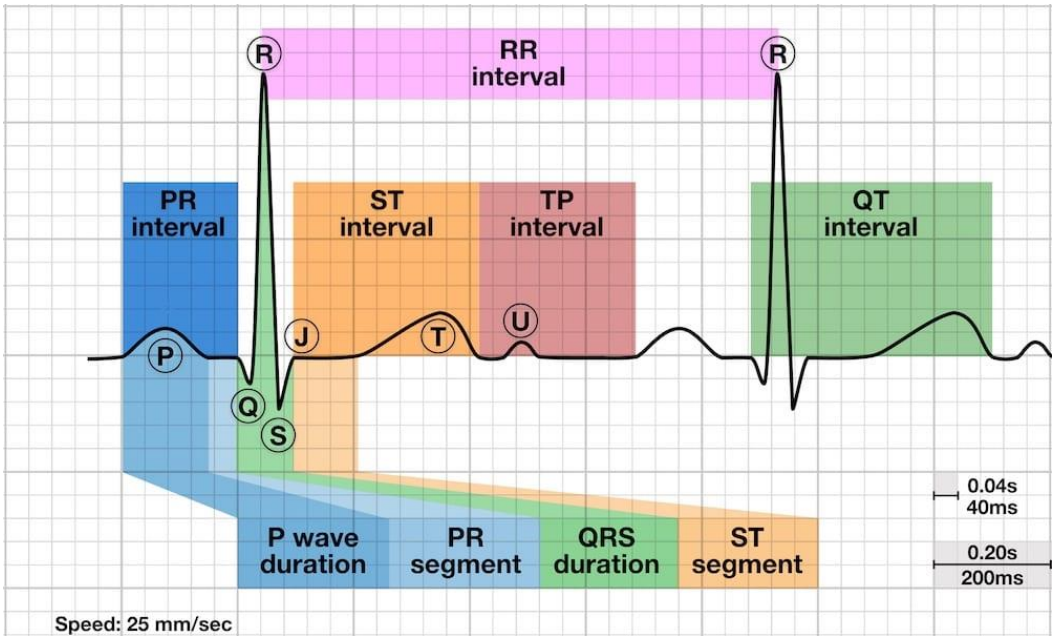

Fig.1.5. ECG of a normal heart with PQRSTUV wave and PR, ST, TP, RR and QT intervals, adapted from [32].

From these various peaks, segments and waves of ECG, R-peak is most commonly used in measuring time interval-based monitoring of BP from PPG waveform.

2. An overview of existing non-invasive blood pressure estimation techniques

Blood pressure can be defined as the pressure that is exercised on the blood vessel wall by the blood that is pumped from the heart. BP can be reported by three parameters namely systolic BP, diastolic BP and mean BP. SBP is the pressure exercised by blood in the last part of the ventricular contraction during systole on the blood vessels wall. DBP is the pressure exercised by blood in the last part of the diastole or expansion. MBP is the measure of rate of average BP exercised on the blood vessels wall [9]. The BP can be measured either invasively or non-invasively. Invasive BP measurement method involves in arterial line placement technique through the radial artery or femoral artery or brachial artery. This method provides the continuous monitoring of BP, but it is quite insecure. Due to injecting, even though the transducer is disposable, it may cause infection. It also causes other risks like bleeding, hematoma, arterial thrombosis and even nerve damage which diminish the advantage of real time measurement of this method. So, the focus of invasive BP measurement is turned towards the non-invasive methods.

2.1. Non-continuous blood pressure monitoring

There are several types of non-invasive BP measurement methods. They may be either continuous or non-continuous. The non-invasive non-continuous BP monitoring consists of Riva-Rocci technique, auscultatory method and oscillometeric method [9]. The Riva-Rocci technique uses an inflatable cuff surrounded by the inelastic material and manometer is included to measure the change in BP. The manual auscultatory method depends on puffing up the cuff using the squeezable bulb to increase the cuff pressure exceeding 120 mm Hg. The stethoscope is placed on the brachial artery. The first sound that is heard is observed as the SBP (phase I) and the sound is termed as Korotkoff sound which is attained by gradually shrinking the cuff and later DBP (phase II) is noted from the sphygmomanometer. The mercury sphygmomanometer performs like the auscultatory method along with that it makes use of a mercury manometer and stethoscope to hear the Korotkoff sounds. Later, the aneroid sphygmomanometer uses a barometer instead of mercury which is then followed by electronic sphygmomanometer that comprises of a pressure gauge and electronic monitor to display the BP [33].

Furthermore, oscillometric method is the technique that measures the BP by estimating the oscillations in the cuff pressure caused by contraction and relaxation of brachial artery. This method also comprises of cuff pressure inflation and deflation above the SBP and below the DBP respectively. The notable difference of this method from the other methods is, it employs a band-pass filter to obtain the oscillometric pulses from the cuff deflation curve which is formed during the deflation of cuff pressure [34].

2.2. Continuous blood pressure monitoring

In recent trends, the non-invasive continuous monitoring has become vital. Hence, Penaz technique came into existence which utilizes the vascular unloading method. It provides the information of changes in blood volume and converts the PPG signal into information of BP. It makes use of infrared light source, photocell and an electro-pneumatic transducer. The infrared light source and the photocell continuously measures the changes in blood volume. During systole, as the blood volume increases, electro-pneumatic transducer controls the cuff pressure by increasing it and hence it expels excess blood volume. During diastole, as the blood volume decreases, electro-pneumatic transducer

furthermore decreases the cuff pressure thereby keeping the blood volume constant. This constant light signal and blood volume leads to the determination of mean arterial pressure which is like the cuff pressure by using the manometer. But this technique is expensive and contains the impacts of change in environmental factor [35]. Another non-invasive continuous arterial pressure measurement is arterial tonometry. This method incorporates a tonometer, pressure transducer and utilizes the bony structure which is below the radial artery. So, the artery is sandwiched between the bone and the tonometer and pressure transducer (see Fig.2.1.). As the tonometer tries to flatten the radial artery, the amount of pressure needed to flatten the artery is measured and the SBP and DBP is measured from that. It provides continuous pulse waveform with the help of strain gauge [36].

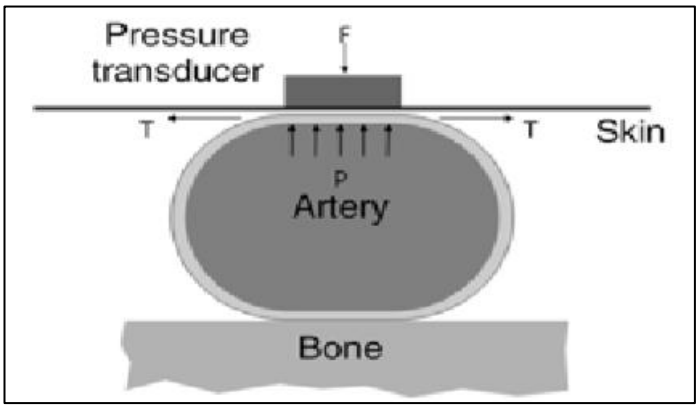

Fig.2.1. Arterial tonometry principle, adapted from [36]

Finapres® (FINger Arterial PRESsure) is the recent technology that enables Penaz techcnique in its equipment with double finger cuff system as a non-invasive continuous BP monitor. It measures SBP, MBP, DBP, heart rate, cardiac output etc. Finometer® is the non-invasive method for beat-to-beat monitoring of BP by using patented modelflow technology. Portapres® (PORTable Arterial PRESsure) is the ambulatory monitor of BP that displays hemodynamic parameters like cardiac output and stroke volume and it can be easily used during exercise while the hand should be stable [37].

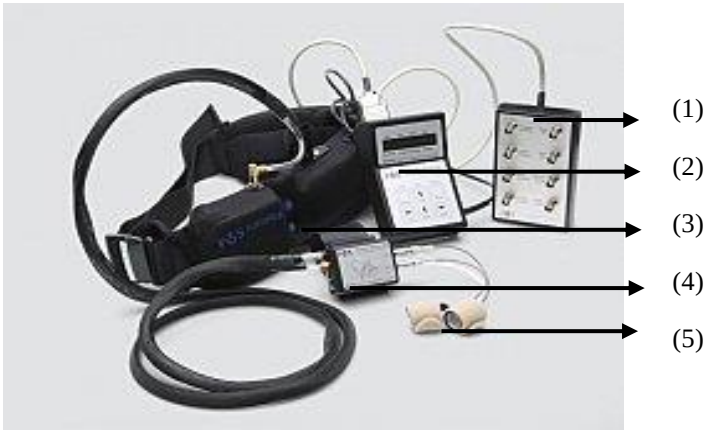

Fig. 2.2. The complete system of Portapres® BP monitoring device, (1) output box, (2) Portapres control unit, (3) main unit to be worn on waist, (4) Front-end unit to be worn on wrist, (5) double finger cuffs, adapted from [37].

But Finapres®, Finometer® and Portapres® are inconvenient for people to use due to its bulk device connections and complexity. Thus, continuous monitoring of BP is vital without causing inconvenience to people to predict the hypertension which is an early indicator of CVD.

2.3. Photoplethysmography based blood pressure estimation techniques

The recent emerging cuff-less non-invasive long-term monitoring of BP parameters based on time interval of PPG waveform includes PTT, PAT, PWV and fiducial points selected for PTT and PAT. The velocity of pulse pressure that transmits from the largest artery to peripheral artery is termed as PWV [15]. When the heart ejects blood from left ventricles, the sudden aortic pressure that travels alongside the artery is absorbed by the arterial walls during systole. Consequently, the arterial pulse wave distributes the energy between arterial walls and arterial blood flow during diastole (see figure 2.3).

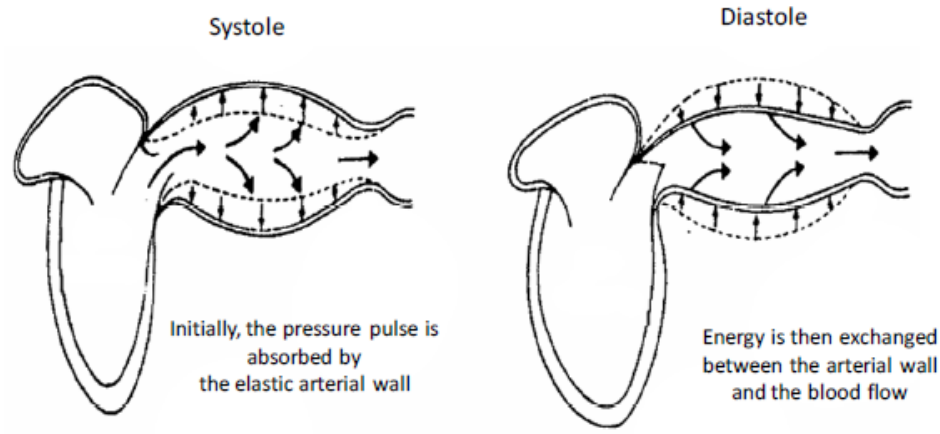

Fig. 2.3. Formation of pulse wave velocity during systole and diastole, adapted from [15].

PWV is clinically used now as a gold standard to measure arterial stiffness non-invasively. PWV can be expressed by combining Bramwell-Hills and Moens-Kortweg's equation [15], [38], [39],

$$A = \frac{L}{Time\ Delay} = \sqrt{\frac{hE_o e^{\propto P}}{\rho d}} \tag{7}$$

where L represents the distance of artery, time delay is the period needed for the pressure wave to reach the periphery of the artery, h is thickness of elastic tube, E_o is Young's modulus for zero arterial pressure, $\propto$ is vessel parameter, P is fluid pressure, ρ is blood density and d is diameter of artery. Time delay can be measured non-invasively using PTT and PAT. An equation to calculate PWV with known length of artery D can be given as:

$$PWV = \frac{D}{PTT} \tag{8}$$

where PTT is the period taken for a pulse to pass on the entire length of artery.

2.3.1. Pulse transit time-based blood pressure estimation

PTT can be calculated [15], [40] by the difference between arrival time of pressure pulse away from the heart i.e. distal limit (PAT_d) and arrival time of pressure pulse near the heart i.e. proximal limit (PAT_p) which is expressed as:

$$PTT = PAT_d - PAT_p \tag{9}$$

The increase in BP in the arteries, eventually increase the PWV which affects the time delay inversely. Thus, greater the BP, lesser the time delay, PTT. PTT or photometric method measures arterial pressure at two different sites which is achieved by the help of PPG i.e. the time period of an arterial pressure trend that arrives at two different locations of blood vessel is measured [9], [41]. In other words, PTT is the time delay between two peaks of two different PPG. Different fiducial points were marked on PTT to estimate BP in various studies. Among them, single fiducial point is considered, and it is called as mean slope transit time (MSTT) which is an alternative to PTT in this study, but this method has limitations and required better performance.

Then, 9 healthy subjects undergone various test to change BP [42]. In that study, SBP and DBP were achieved from lead V5 ECG and left finger PPG concurrently with the help of cuff sphygmomanometer placed on the right wrist. Five fiducial points of PPG were selected, and they are correlated with SBP and PP. The results shown that fiducial points, time and area ratio of systole to diastole, time distance of PPG and diastolic interval could advance the functioning of PPG-based BP estimation. The foot of PTT has higher correlation to invasive DBP while the PPG peaks are unpredictable markers of SBP.

In the study [43], the variation in pulse wave and baseline wander in pressure for long-term PTT-based BP monitoring is examined. The five characters of pulse wave: heart cycle (HC), diastolic time (DIT), systolic (SA), position of local minimum of the first derivative wave (PMID) and height of tidal wave peak (HTWP) has shown the changes during change in pressure baseline which were the better indicators. Likewise, another study [44] which observed 22 healthy individuals for BP estimation using intensity ratio of first derivative wave of PPG (1^{st} dPIR) and PTT has increased accuracy. 1^{st} dPIR also shown that its output is baseline wander free and low-frequency noise free signals.

2.3.2. Pulse arrival time-based blood pressure estimation

PAT is the time difference between the R-peak of ECG and a distal arterial wave i.e. any fiducial point of PPG and is equivalent to the total amount of PTT and pre-ejection period (PEP) [38], [40], [41]. PEP represents the period required to unlock aortic valve from isovolumetric contraction of heart.

$$PAT = PTT + PEP \tag{10}$$

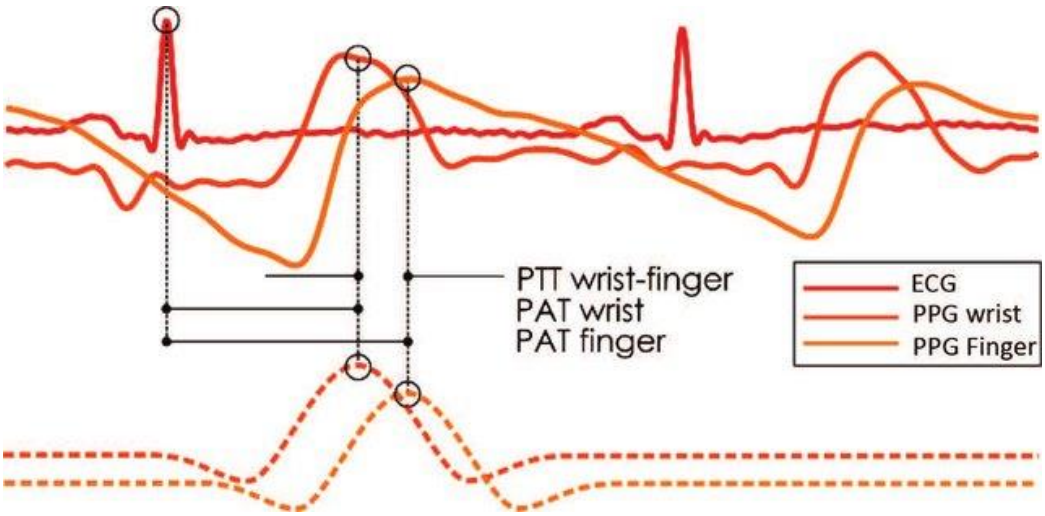

Fig. 2.4. PAT wrist taken from PPG on wrist and ECG, PAT finger taken from PPG on finger and ECG, PTT derived from difference between PAT wrist and PAT finger, adapted from [41] .

PAT better represents SBP due to the ventricular contraction and vascular function dependency rather than DBP and MBP. This result is even proved in another study [40] which states that PAT estimation correlates better with SBP rather than DBP. In the comparison study [45], six foot finding methods were chosen among which the maximum value in the PPG wave and the minimum value in the PPG wave were time-based methods. It is seen that the minimum value in the PPG wave is obviously near the base of the pulse wave whereas maximum value arises later in the cardiac cycle. Later on, PAT calculation is done by using various PPG feature detection methods such as, PAT peak- largest value of a single PPG waveform, PAT foot- smallest value of a single PPG waveform, PAT dpeak- largest value of the first derivative of a single PPG waveform, PAT ddpeak-maximaum value of second derivative of a single PPG waveform [10]. The results shown that the PAT dpeak has given the lowest variance in PAT and in the difference of standard deviation of PP and RR intervals while the ddpeak and PAT foot has given nearly alike results.

2.3.3. Photoplethysmogram derivative-based blood pressure estimation

PPG derivatives are most likely to be either first derivative of PPG or second derivative of PPG. The second derivative of PPG (SDPTG) were observed for 30 subjects and they divided according to their age [46]. The SDPTG-AI which is the second derivative of PPG with ageing index is employed and the wave consists of initial positive wave (a wave), early negative wave (b wave), re-upsloping wave (c wave), late re-down sloping wave (d wave) and diastolic positive wave (e wave). Here b/a, d/a and SDPTG-AI parameters have shown difference for different age subjects and it is helpful to determine the condition of artery. First derivative of PPG would likely be a good predictor for arterial stiffness whereas the second derivative of finger PPG has the better performance than first derivative of PPG [47].

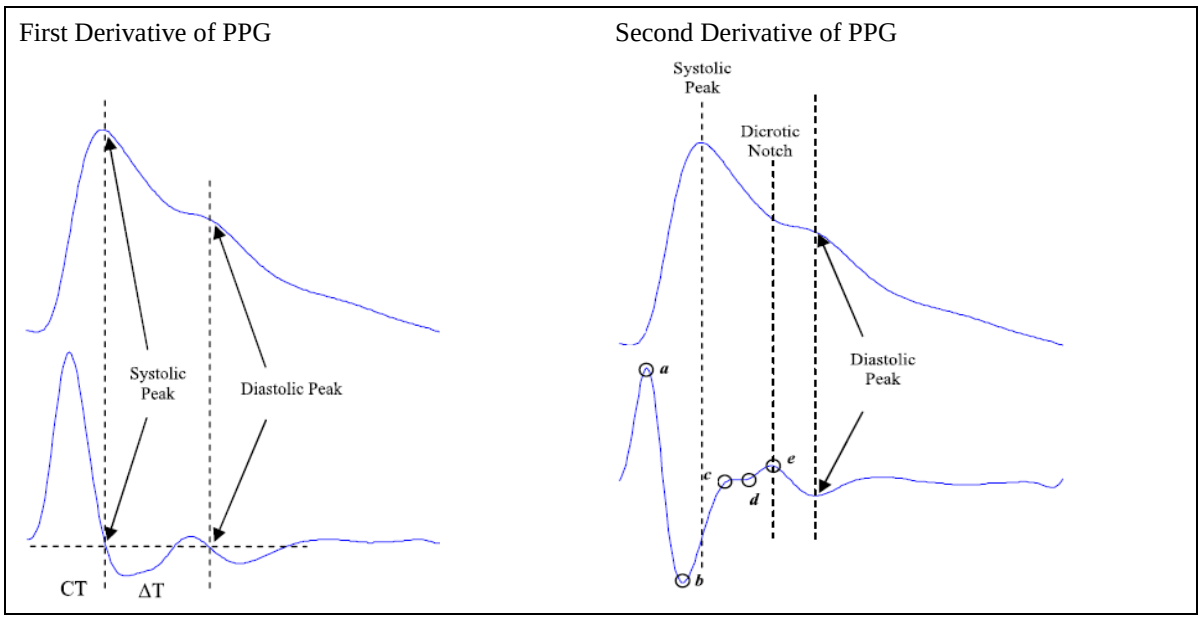

Fig.2.5. (a) Top figure shows the PPG wave and bottom figure shows the first derivative of PPG with systolic and diastolic peak markings. CT-crest time-time from foot of PPG to peak of PPG, ΔT-time between systolic and diastolic peak. **(b)** Top figure shows PPG wave and bottom figure shows second derivative of PPG with selected fiducial points a, b, c, d and e, adapted from [47].

Second derivative of PPG provides the valuable prediction of coronary heart disease and atherosclerosis by providing the near correlation with the distensibility of carotid artery. The increased arterial stiffness leads to raised b/a index and decreased c/a, d/a and e/a indices. Among the six-foot finding methods, maximum first derivative, maximum second derivative, intersecting tangents diastole patching in the study [45] were based on the derivates measurement. From these methods, the results shown that the best method for achieving immediate measurement of pulse rate from PPG signals is intersecting tangent method.

3. Databases of physiological signals

This chapter consists of five sections such as acquiring the physiological signals like PPG, ECG and BP (see section 3.1), experimental procedure handled and physiological conditions of volunteers for thermal stress test database (see section 3.2) and breathing test database (see section 3.3) and finally pre-processing of physiological signals and statistical analysis of the signals in sections 3.4 and 3.5 respectively.

3.1. Acquisition of physiological signals

PPG is acquired by Nautilus1 (BMII, Lithuania) while non-invasive continuous blood pressure measurement and recording system Portapres Model-2 (Finapres Medical Systems B.V., Netherlands) was used for acquiring continuous arterial BP. ECG was recorded by standard Einthoven leads (I, II, and III leads) whereas PPG was recorded from right hand. In this thesis, all the signals were upsampled to 1000 Hz. In breathing test database, ECG was acquired by KTU BMII Cardiologor V6 device while Nautilus 1(BMII, Lithuania) is used for acquiring ECG in thermal stress test database.

3.2. Thermal stress test database

The thermal stress test has been conducted to determine how thermal stress produced in the evening by means of sauna affects the mental activity at night and the functional efficiency of cognitive and neuro-muscular system and the hormonal change in the morning [48]. This study was conducted in collaboration with partners from Lithuanian Sports University. The experiment was divided into three steps such as experiment no.1, experiment no.2 and control no.1 each lasted up to 54 hours. The protocol was permitted by Kaunas Regional Biomedical Research Ethics Committee.

Out of 15 healthy male volunteers, first 4 volunteers were used in this thesis. The volunteers were non-smokers, normotensive and not intaking any medication throughout the study. They have been instructed to cease exercise for 54 hours, food for 6 hours and other beverages like coffee, energy drinks, etc. for 12 hours before the examination. The selected volunteer's physiological characteristics is presented in Table 1. This thesis uses the signals from control no.1.

Table 1. Physiological characteristics of the volunteers. BMI* - Body Mass Index, adapted from [48]

Volunteer	Age (years)	Sex	Height (cm)	Weight (kg)	Bmi*(kg/m^2)
Volunteer no.1	28	Male	183	69.7	20.8
Volunteer no.2	35	Male	183	82.0	24.5
Volunteer no.3	28	Male	190	88.1	24.4
Volunteer no.4	26	Male	187	80.1	22.9

The sauna room temperature was set to 80-90°C, relative humidity to 30%. The subjects were allowed to sit before and after the sauna sessions in the neutral temperature of 25°C.

REST 1	Sauna session 1	REST 2	Sauna session 2	REST 3	Sauna session 3	REST 4	Sauna session 4	REST 5

00:00 00:20 00:35 00:50 01:00 01:15 01:25 01:40 01:50 02:20

Fig.3.1. Experimental protocol of thermal stress test database, adapted from [48]

ECG, PPG, ACC and temperature signals were recorded during the entire experiment while BP is recorded only at rest period: Rest 1 – 20 min., Rest 2 – 10 min., Rest 3- 10 min., Rest 4 – 10 min., Rest 5 – 30 min. In this thesis, Rest 2 to Rest 5 is utilized to observe the highest changes in BP waveform. Hence the total time period used here is 2 hours and 20 minutes. This database can be used to find the correlation of BP with PAT and one rest session can be used to create the model and the other can be used to test the model.

3.3. Breathing test database

The breathing test was conducted to observe the change in BP during exercises such as Valsalva manoeuvre and full controlled respiration. This test was carried out for 8 healthy male volunteers and 2 healthy female volunteers. However, two sets of signals were not able to be synchronized properly and BP signals of three volunteers had been corrupted by calibration for every 10 seconds. Hence 4 healthy male volunteers and 1 female volunteer is used in this thesis (see Table 2). The volunteers were instructed to be in rest position in a chair without any external disturbances.

Table 2. Physiological characteristics of volunteers of respiratory test

Volunteer	Age (years)	Sex	Height (cm)	Weight (kg)
Volunteer no.1	28	Male	183	69.7
Volunteer no.2	20	Male	172	60.0
Volunteer no.3	19	Male	170	61.2
Volunteer no.4	18	Male	168	63.5
Volunteer no.5	18	Female	165	65.0

The experiment was conducted in continuous two phases for about 16 minutes. Initial phase was carried out at 5 minutes of rest followed by Valsalva manoeuvre in which the volunteer's nostrils and mouth were closed and they try to exhale for 20 seconds, next the continuous second phase is 5 minutes of rest, full controlled respiration where the volunteers were instructed to deep breath in for 5 seconds and breath out for next 5 seconds and the procedure continues for 1 minute which is followed by final 5 minutes of recovery time.

Rest Session	***Valsalva manoeuvre***	Rest Session	***Full controlled Respiration***	Recovery Period

00:00:00 00:05:00 00:05:20 00:10:20 00:11:20 00:16:00

Fig.3.2. Experimental protocol of breathing test.

During the whole procedure, ECG, PPG and BP signals were recorded. In this thesis, the period of Valsalva manoeuvre and full controlled respiration is utilized to test and predict BP parameters and their correlation with desired algorithms.

3.4. Pre-processing

The collected stress test database and respiratory test database were analysed using various signal processing methods such as: pre-processing the signals, finding fiducial points of PPG (middle amplitude of PPG slope, peaks of SSF and finding the peaks of PPG using matched filter). Initially, in the stress test database, PPG signal whose sampling rate is 1000 Hz is pre-processed by a butterworth low pass filter with cut off frequency 27 Hz and butterworth high pass filter with cut off frequency 0.4 Hz which removes the baseline wander. ECG signal is band pass filtered at the frequency range of 0.4 to 30 Hz using butteworth filter to avoid baseline contamination and a rejection filter is applied to remove 50 Hz powerline interference.

Later, for the respiratory test database, PPG signal of sampling frequency 1000 Hz is filtered using a butterworth low pass filter and high pass filter at a cut off frequency 0.5 Hz and 25 Hz respectively to remove baseline wander. ECG signal with sampling frequency 1000 Hz was low pass filtered by enabling Parks-McClellan optimal FIR filter whose passband frequency is 35 Hz, stopband frequency is 50 Hz and attenuated by passband ripple and stopband ripple at the rate of 0.00575 dB and 0.0001 dB respectively with a density factor of 20. Afterwards, ECG is removed with low frequency noises by butterworth high pass filtering at a cut off frequency 0.5 Hz. Portapres and Cardiologer synchronization problems on breathing test database were solved by using analog output from Portapres for event generation in Cardiologer (see Fig. 3.3).

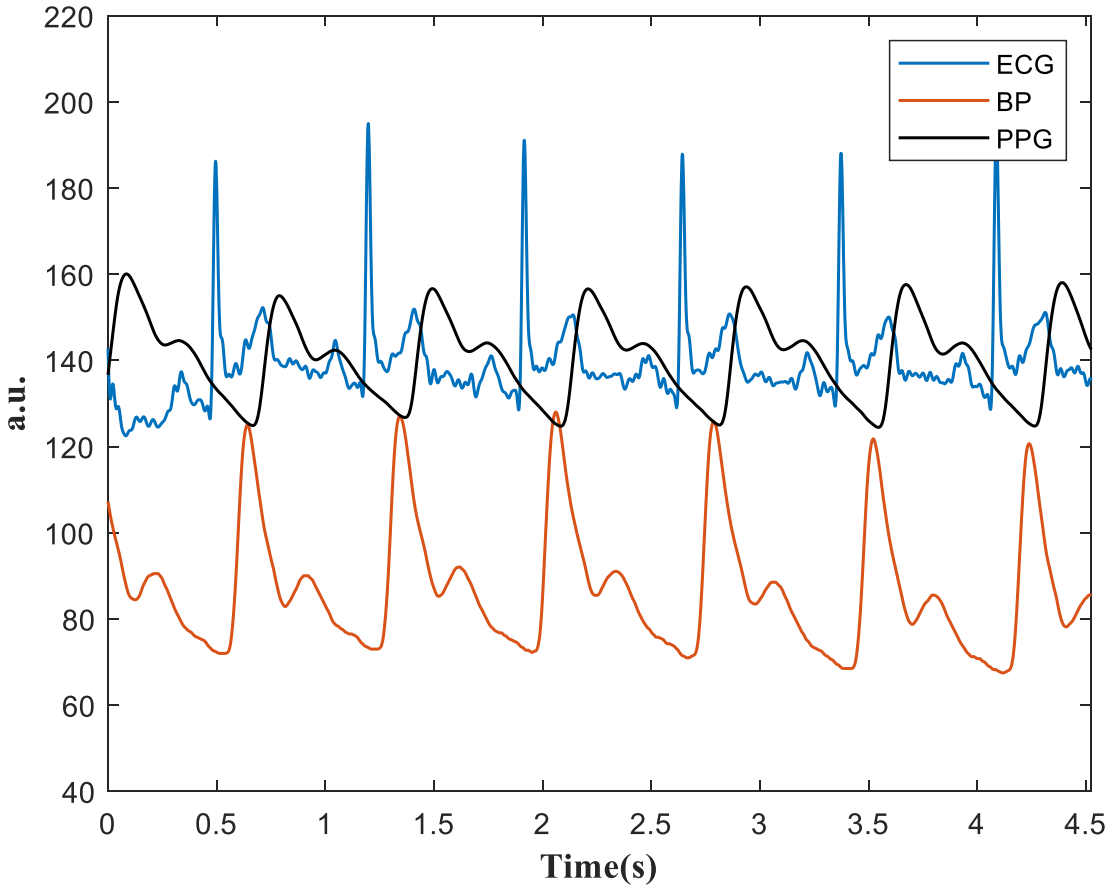

Fig.3.3. Example of pre-processed ECG, BP and PPG signals for volunteer 1 from breathing test database.

3.5. Statistical analysis

Pearson correlation coefficient is used to find how one variable is correlated or related on another variable. The level of strength of Pearson correlation coefficient *r* can be seen in Table 3 based on which the correlation coefficients will be defined in upcoming results. The colour of each strength level would indicate the respective correlation coefficient. So that, purple for very strong correlation, pink for strong correlation, blue for moderate correlation, green for weak correlation and yellow for very weak correlation.

Table 3. Level of Strength for Pearson correlation coefficients

Level of strength	**Correlation coefficients (r values)**
Very strong	0.80-1.00
Strong	0.60-0.79
Moderate	0.40-0.59
Weak	0.20-0.39
Very weak	0.00-0.19

4. Methods

This chapter consists of four sections, first section 4.1 takes the detection of R-peaks in ECG, second section 4.2 has three methods that are selected to find fiducial points of PPG such as middle amplitude of PPG in sub-section 4.2.1, peaks of slope sum function in sub-section 4.2.2, peaks of matched filter in sub-section 4.1.3, third section 4.3 explains the detection of SBP, DBP, MBP and PP and forth section 4.4 has two models that are used to estimate BP such as Moens-Korteweg model and derivative of Moens-Korteweg and linear model of vascular elasticity model.

4.1. R-peaks detection in electrocardiogram

R-peak detection of ECG requires extraction of QRS complex whose frequency range is between 12 and 20 Hz and it is achieved by applying a butterworth filter of this required frequency range. Afterwards the extracted signal is integrated by taking the absolute value of signal followed by smoothing of signals using another butterworth low pass filter at 13 Hz of cut off frequency to remove high frequency noises. Threshold is pre-set with initial maximum of ECG and it is established as adaptive to the forthcoming R-peaks. To detect peaks, the algorithm checks for peaks within 1.5 seconds in every cardiac cycle for the given threshold, if the peak is not detected, the threshold adapts itself to the lower value and checks for lower R-peaks. Next, the indices of R-peaks and their respective amplitudes were extracted and stored for further processing of the study (see Fig. 4.1(a)).

4.2. Methods for finding fiducial points of photoplethysmogram in pulse arrival time estimation

The fiducial points of PPG considered are peaks and middle amplitude of upslope of pulses in PPG. The middle amplitude of PPG slope (see subsection 4.2.1), peaks of slope sum function (see subsection 4.2.2) and peaks of matched filtered PPG (see subsection 4.2.3) are chosen as the three fiducial points of PPG. The calculated fiducial points are then subtracted from R-peaks of ECG to get their respective PAT values.

4.2.1. Middle amplitude of pulse slope

The middle amplitude of pulse slope is defined by the middle value of the amplitude of PPG upslope which will be 50% or average of peak and foot of PPG signal [13]. At the beginning the high frequency noises of PPG is attenuated by low pass FIR filter at a cut off frequency 10 Hz. The upslope of PPG is initially found within the range of two subsequent R-peaks indices or RR interval (R_i, where i is the index of R-peak) of ECG and the cycle waits for every 150 milliseconds and the cycle repeats for the length of R-peak indices. The maximum value of upslope is recorded as peak of PPG S_p and it is expressed as:

$$s_p = \underset{s\epsilon[R_i,R_{i+1}]}{\arg\max}\{x(s)\} \tag{11}$$

Where $x(s)$ is pre-processed PPG signal. In the same upslope, minimum value within the range of R_i and S_p is noted as foot of PPG S_f and given as:

$$s_f = \underset{s\epsilon[R_i,S_p]}{\arg\min}\{x(s)\} \tag{12}$$

Subsequently, middle amplitude points of PPG slope S_m which is the point between S_p and S_f where the 50% of amplitude of maximum of pulse amplitude is achieved can be expressed as:

$$s_m = \underset{s\epsilon[s_p, s_f]}{\arg\min} \left\{ \left| x(s) - \frac{x(s_p)+x(s_f)}{2} \right| \right\} \tag{13}$$

$PAT_{Slope50}$ for every cardiac cycle $PAT_{Slope50i}$ is calculated which is the time difference between the timing of middle amplitude of PPG slope S_m, $Slope50_{pi}$ and its subsequent time instant of R-peak index, ECG_{Ri} (see Fig. 4.1(b)).

$$PAT_{Slope50i} = Slope50_{pi} - ECG_{Ri} \tag{14}$$

4.2.2. Peaks of slope sum function

The SSF helps to improve the upslope of the PPG signal and dominate the rest of the signal. This technique simplifies the identification of peaks of PPG. At first, a low pass FIR differentiator of order 256 is designed with transition band between 7.7 Hz and 8 Hz for pre-processed PPG signal. The delay of the differentiator is the half of the filter order and it is removed after filtration. Then negative derivative samples are changed to zero. Now the SSF is implemented at time t, SSF(t) which can be given as follows:

$$SSF(t) = \sum_{n=t-w}^{t} Q_n \,,\; Q_n = \begin{cases} P_n, & P_n > 0 \\ 0, & P_n \leq 0 \end{cases} \tag{15}$$

where w is the length of the considering window, Q_n is the output from differentiator and P_n is the nth sample of filtered PPG signal. Here w is chosen to be 54 samples or 108 milliseconds which is the time interval of the upslope of the PPG signal [12]. Then the peaks of SSF is calculated within their subsequent RR interval, RR_i. PAT_{SSF} for every cardiac cycle PAT_{SSFi} is calculated which is the time difference between the timing of peak of slope sum function, SSF_{pi} and its subsequent time instant of R-peak index, ECG_{Ri}.

$$PAT_{SSFi} = SSF_{pi} - ECG_{Ri} \tag{16}$$

SSF and the respective peaks are illustrated in Fig. 4.1(c).

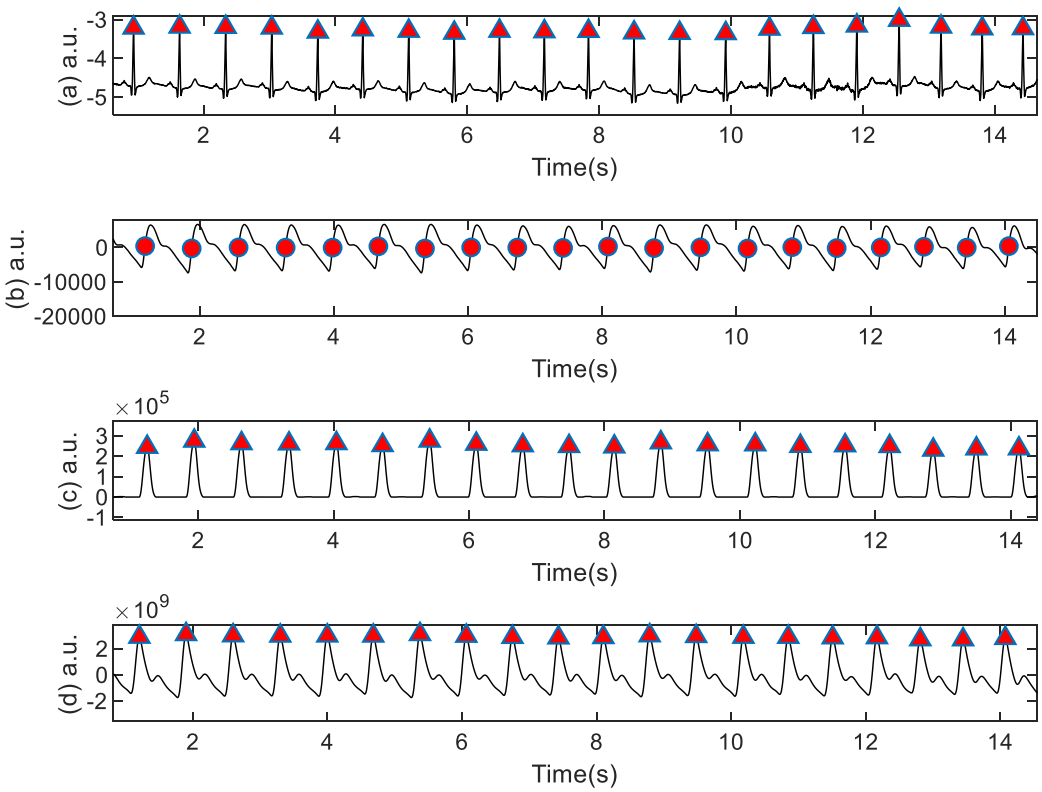

Fig. 4.1. Provided results from thermal stress test database: (a) ECG with R peaks, (b) PPG with middle amplitude of PPG signal, (c) SSF with peaks of SSF and (d) Matched filtered PPG with its peaks.

4.2.3. Peaks of matched filtered photoplethysmogram

The matched filter finds the match for the similar pattern from the pre-defined waveform or the template of the selected pattern of the original PPG signal in the time sequence [14]. The defined template is the initial upslope of PPG i.e. within the range of first foot, S_{fa} (a is the index of foot) and first peak, S_{pb} (b is the index of peak). Then conjugate is taken for the defined template. This conjugated template *h(t)* is now convoluted with pre-processed PPG signal *x(k)* which provides matched filtered signal. Delay is half the length of conjugated template and later it is removed from the matched filtered signal *y(t)*. The matched filter can be expressed as:

$$y(t) = \sum_{t=0}^{K-t} h(t)x(k-t) \tag{15}$$

The matched filtered signal provides higher amplitude to the matched patterns in which the time sequence looks like template and in other places with lower amplitude. This simplifies the way to find the peaks of PPG pulse. The peaks of matched filtered signal are evaluated within the RR interval, R_i. PAT_{Match} for every cardiac cycle PAT_{Matchi} is calculated which is the time difference between the timing of peak of matched filtered PPG, $Match_{pi}$ and its subsequent time instant of R-peak index, ECG_{Ri}. (see Fig. 4.1(d)).

$$PAT_{Matchi} = Match_{pi} - ECG_{Ri} \tag{16}$$

4.3. Detection of systolic and diastolic blood pressure in blood pressure signal

The maximum peak of blood pressure waveform is detected to be SBP. The peak of SBP is calculated within the RR interval, R_i which can be expressed as (17).

$$SBP_j = \underset{n\epsilon[R_i,R_{i+1}]}{\arg\max}\{x(n)\} \tag{17}$$

where $x(n)$ is the BP signal. The minimum value or the foot of blood pressure waveform is DBP calculated within R_i by giving an approximate minimum value j for every SBP which then checks for the minimum value DBP_j than j and it should not be equal to previous SBP.

$$DBP_j = \underset{n\epsilon[R_i,SBP_j]}{arg\ min}\{x(n)\} \tag{18}$$

PP and MBP is calculated from detected SBP and DBP where PP is the subtraction of DBP from SBP and MBP is estimated as the equation (3).

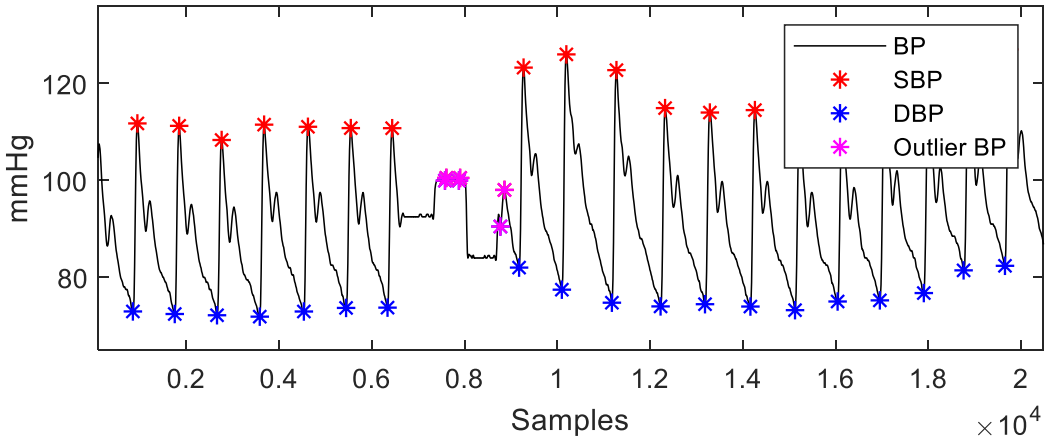

Fig. 4.2. SBP and DBP with outliers of BP

The outliers of SBP and DBP were removed when PP is less than 20 mmHg. The outlier is due to the calibration of Portapres for every 70 seconds. The other outliers which is due to PAT were also removed by providing thresholds. Fig.4.2 and 4.3 shows the outliers of BP plotted on BP and without outliers of BP respectively.

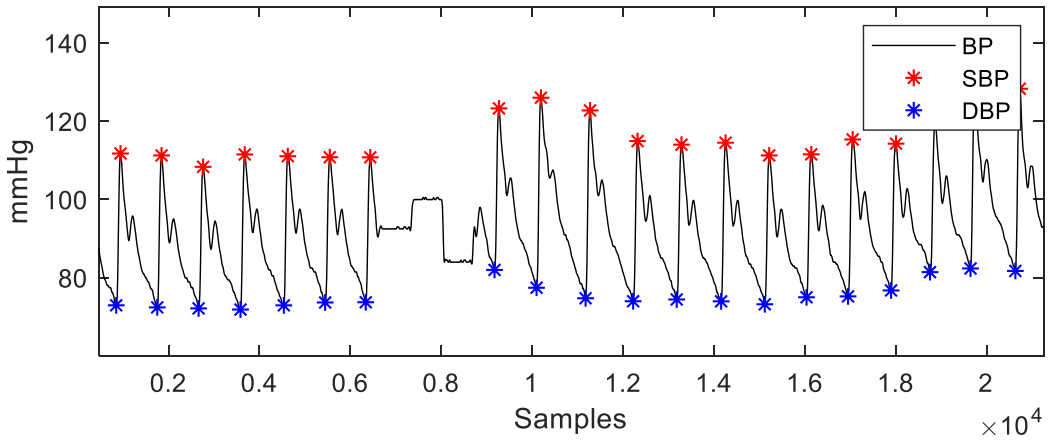

Fig. 4.3. SBP and DBP without outliers of BP

4.4. Pulse arrival time-based models for estimating blood pressure parameters

The vascular elasticity models for BP based on PAT values are divided into two types:

- Linear models
- Non-linear models

The non-linear vascular elasticity models are further sub-divided into Moens-Korteweg and exponential arterial elasticity (MK) model [49], Moens-Korteweg and Bramwell-Hill model and MBP developed Moens-Korteweg and Bramwell-Hill model whereas the linear vascular elasticity model is derivative of Moens-Korteweg and linear (L-DMK) model [50]. This project mainly focuses on MK model and L-DMK model of vascular elasticity model. Initially the model is used to find the estimated or real BP parameter. The coefficients of the estimated BP parameters then used to predict the BP parameter of next session in thermal stress test database and to predict the BP parameter of next phase of breathing test database.

Moens-Korteweg and exponential arterial elasticity model and derivative of Moens-Korteweg and linear model can be expressed as below:

$$MK = x(1) \times \ln(PAT) + x(2) \tag{17}$$

$$L - DMK = x(1) + x(2) \times \ln(PAT) \tag{18}$$

where *x(1)* and *x(2)* are the coefficients of estimated BP parameters, MK is the predicted value of BP parameters for Moens-Korteweg model and L-DMK is predicted value of BP parameters for derivative of Moens-Korteweg and linear model.

5. Results and Discussions

This chapter consists of all the results and discussions about PAT values that are estimated for thermal stress test database in section 5.1 and PAT values that are estimated for breathing test database in section 5.2.

5.1. Estimation of blood pressure parameters in thermal stress test database

BP is an early indicator of many diseases as mentioned in the previous studies [5]–[8], therefore it is mandatory to have a long-term monitoring method of BP. This thesis has concentrated on various methods to find PAT which includes middle amplitude of PPG slope, peaks of slope sum function and peaks of matched filtered PPG. The PAT values of thermal stress test database were calculated which provided $PAT_{Slope50,}$ PAT_{SSF} and PAT_{Match} and they are illustrated in Fig. 5.1. PAT_{SSF} amplitude is varying from 300 ms to 280 ms which is a good variation. $PAT_{Slope50}$ and PAT_{Match} also have the good variation such as from 260 ms to 240 ms for PAT_{Match} and from 240 ms to 220 ms for $PAT_{Slope50}$.

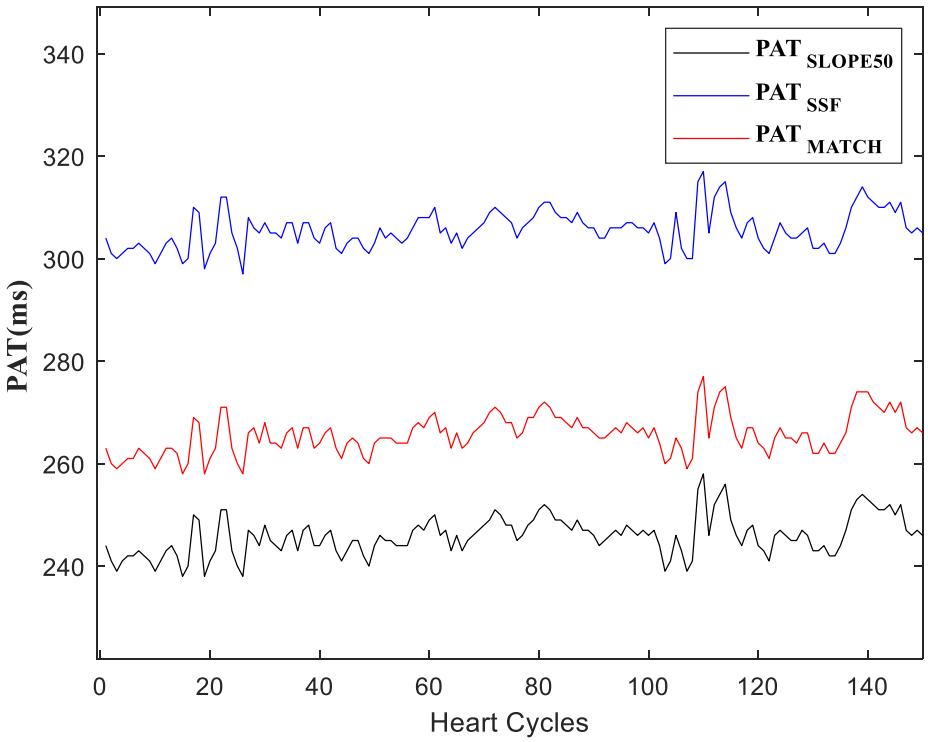

Fig. 5.1. $PAT_{Slope50}$, PAT_{SSF}, PAT_{Match} for the volunteer no.4 from thermal stress test database.

The correlation coefficients of rest session 2, rest session 3 and rest session 4 were provided on table 4, table 5 and table 6 respectively which shows the three PAT methods correlation with BP parameters through Pearson correlation coefficient *r*.

Table 4. Rest session 2 for thermal stress test database: SBP, DBP, MBP and PP correlation with PAT values shown through correlation coefficient *r*.

Volunteer	PAT_{Match} (*r* values)				$PAT_{Slope50}$ (*r* values)				PAT_{SSF} (*r* values)			
	SBP	MBP	DBP	PP	SBP	MBP	DBP	PP	SBP	MBP	DBP	PP
1	0.1729	0.1937	0.1886	0.1001	0.2018	0.1928	0.1608	0.1639	0.1210	0.1105	0.0873	0.1056
2	-0.3801	-0.4430	-0.4837	-0.2743	-0.4310	-0.4851	-0.5102	-0.3316	-0.4111	-0.4584	-0.4772	-0.3214
3	-0.4655	-0.0897	0.1576	-0.6407	-0.4299	-0.0541	0.1860	-0.6274	-0.4875	-0.1264	0.1196	-0.6308
4	-0.5006	-0.3831	-0.3077	-0.4399	-0.4907	-0.3650	-0.2861	-0.4636	-0.5237	-0.4130	-0.3400	-0.4223

From the Table 4 we can see that volunteer 1 is having very weak correlation, volunteer 2 has downhill moderate and weak correlation, volunteer 3 has downhill strong, moderate and weak correlation and finally volunteer 4 has downhill moderate and weak correlation. It is noted that SBP is having downhill moderate correlation with all PAT methods such that correlation coefficient is *r = -0.4655* and *r = -0.5006* for volunteer 3 and 4 respectively with PAT_{Match}, *r = -0.4310*, *r = -0.4299* and *r = -0.4907* for volunteer 2, volunteer 3 and volunteer 4 respectively with $PAT_{Slope50}$ and finally *r = -0.4111*, *r = -0.4875* and *r = -0.5237* for volunteer 2, volunteer 3 and volunteer 4 respectively with PAT_{SSF}. MBP does not have noticeable correlation except for volunteer 2 with *r = -0.4430* for PAT_{Match}, *r = -0.4851* for $PAT_{Slope50}$ and *r = -0.4111* for PAT_{SSF} showing as downhill moderate correlation and volunteer 4 has moderate downhill correlation as *r = -0.4310* only for PAT_{SSF}. Then DBP is also having moderate downhill correlation for volunteer 2 with *r = -0.4837*, *r = -0.5102* and *r = -0.4772* for PAT_{Match}, $PAT_{Slope50}$ and PAT_{SSF} respectively. Later, PP is having downhill strong correlation for volunteer 3 with *r = -0.6407*, *r = -0.6274* and *r = -0.6308* and for volunteer 4 with *r = -0.4399*, *r = -0.4636* and *r = -0.4223* for PAT_{Match}, $PAT_{Slope50}$ and PAT_{SSF} respectively. It is observed from rest session 2 that for all methods, SBP and PP is having moderate and strong correlation compared to DBP and MBP which is having very weak correlation.

Table 5. Rest session 3 for thermal stress test database: SBP, DBP, MBP and PP correlation with PAT values shown through correlation coefficient r.

Volunteer	PAT_{Match} (*r* values)				$PAT_{Slope50}$ (*r* values)				PAT_{SSF} (*r* values)			
	SBP	MBP	DBP	PP	SBP	MBP	DBP	PP	SBP	MBP	DBP	PP
1	-0.2381	-0.2611	-0.2768	-0.1848	-0.2033	-0.2249	-0.2404	-0.1545	-0.2337	-0.2561	-0.2712	-0.1818
2	0.1645	0.0847	-0.0190	0.2589	0.1853	0.1082	0.0064	0.2746	0.1447	0.0638	-0.0400	0.2419
3	-0.3137	-0.3156	-0.2779	-0.2618	-0.2362	-0.2380	-0.2099	-0.1968	-0.3698	-0.3738	-0.3310	-0.3065
4	-0.8337	-0.8709	-0.8506	-0.4416	-0.8406	-0.8689	-0.8424	-0.4665	-0.8411	-0.8786	-0.8580	-0.4458

The rest session 3 does not have noticeable correlation with all BP parameters as it has shown only weak and very weak correlation for volunteers 1, 2 and 3. The only exception is volunteer 4 who has downhill very strong downhill correlation for SBP as *r = -0.8337*, *r = -0.8406* and *r = -0.8411*, for MBP as *r = -0.8709*, *r = -0.8689* and *r = -0.8786* and finally for DBP as *r = -0.8506*, *r = -0.8424* and *r = -0.8580* for PAT_{Match}, $PAT_{Slope50}$ and PAT_{SSF} respectively. Also volunteer 4 has moderate

downhill correlation for PP such as *r = -0.4416* with PAT_{Match}, *r = -0.4665* with $PAT_{Slope50}$ and *r = -0.4458* with PAT_{SSF}. From rest session 3, it is noted that only one volunteer is having very strong downhill correlation for SBP, MBP and DBP and moderate downhill correlation for PP while other volunteers shows only weak and very weak correlation.

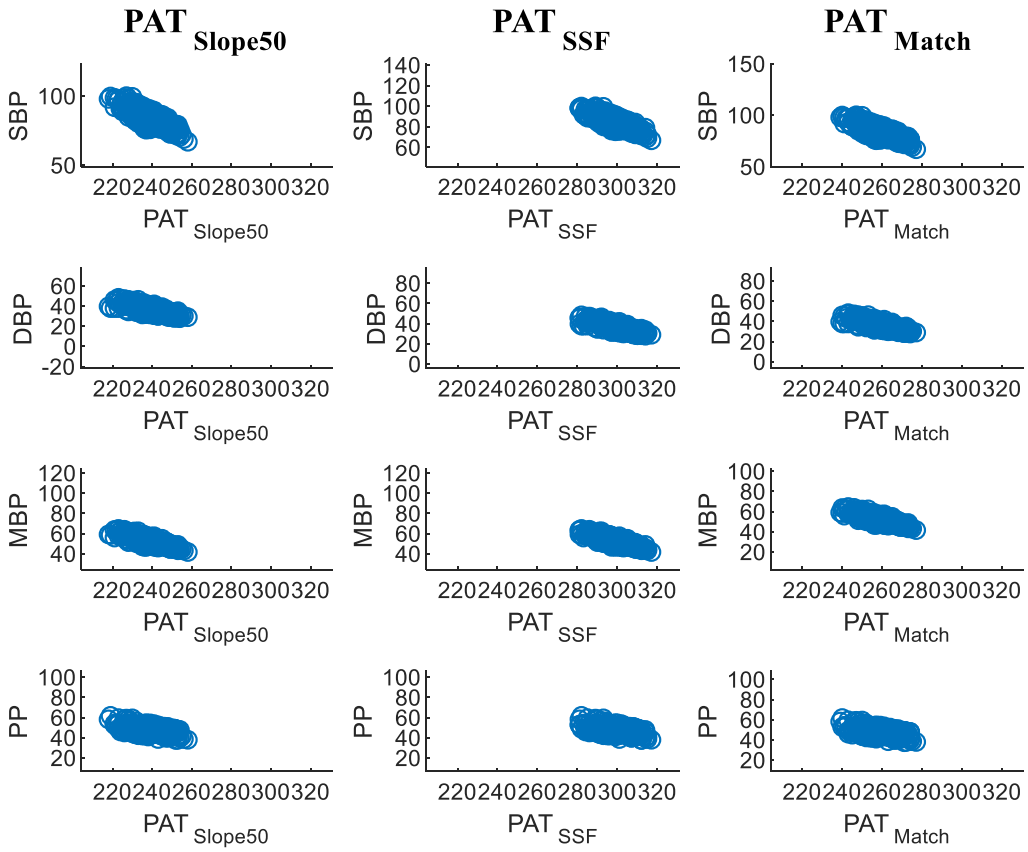

Fig. 5.2. Scattered plot of SBP, DBP, MBP and PP with PAT values for rest session 3, volunteer no.4.

As the Table 5 shows, it is clearly seen in scatter plot (see Fig. 5.2) that volunteer 4 has very strong downhill correlation with SBP, MBP and DBP and moderate downhill correlation with PP.

To test the estimated models, at first, rest session 2 was used to create MK model and L-DMK model for SBP and then tested on rest session 3. The correlation between real SBP and predicted SBP is expressed by Pearson correlation coefficients. Volunteers 1 and 3 has weak correlation while volunteer 2 has very weak correlation. In contrast, volunteer 4 has very strong uphill correlation of SBP such as *r = 0.8334* and *r = 0.8402* for PAT_{Match}, *r = 0.8402* and *r = 0.8337* for $PAT_{Slope50}$ and *r = 0.8334* and *r = 0.8402* for PAT_{SSF} when tested on MK and L-DMK model respectively.

From Table 6 it is observed that volunteers 1 and 2 have downhill correlations while volunteers 3 and 4 have uphill correlation. This variation for volunteers is may be due to the synchronization of Portapres device. Bland-Altman plot is plotted to see the difference of agreements between SBP real and SBP predicted which was created by MK model and L-DMK model for PAT_{Match} on rest session 2 and rest session 3 for predicting which is shown in Fig. 5.3.

Table 6. Models created on rest session 2 for SBP and tested on rest session 3 and their real and predicted SBP correlation with PAT methods.

Volunteer	MK Model			L-DMK Model		
	PAT_{Match} (*r* values)	$PAT_{Slope50}$ (*r* values)	PAT_{SSF} (*r* values)	PAT_{Match} (*r* values)	$PAT_{Slope50}$ (*r* values)	PAT_{SSF} (*r* values)
1	-0.2419	-0.2083	-0.2371	-0.2381	-0.2033	-0.2337
2	-0.1646	-0.1853	-0.1448	-0.1645	-0.1853	-0.1447
3	0.3115	0.2346	0.3673	0.3137	0.2362	0.3698
4	0.8334	0.8402	0.8409	0.8337	0.8406	0.8411

The mean difference is of MK model is -3.2847 mmHg and L-DMK model is -3.1805 mmHg and their Pearson correlation coefficient are *r =0.8334* for MK model and *r = 0.8337* for L-DMK model which is a very strong uphill correlation as illustrated in Table 6.

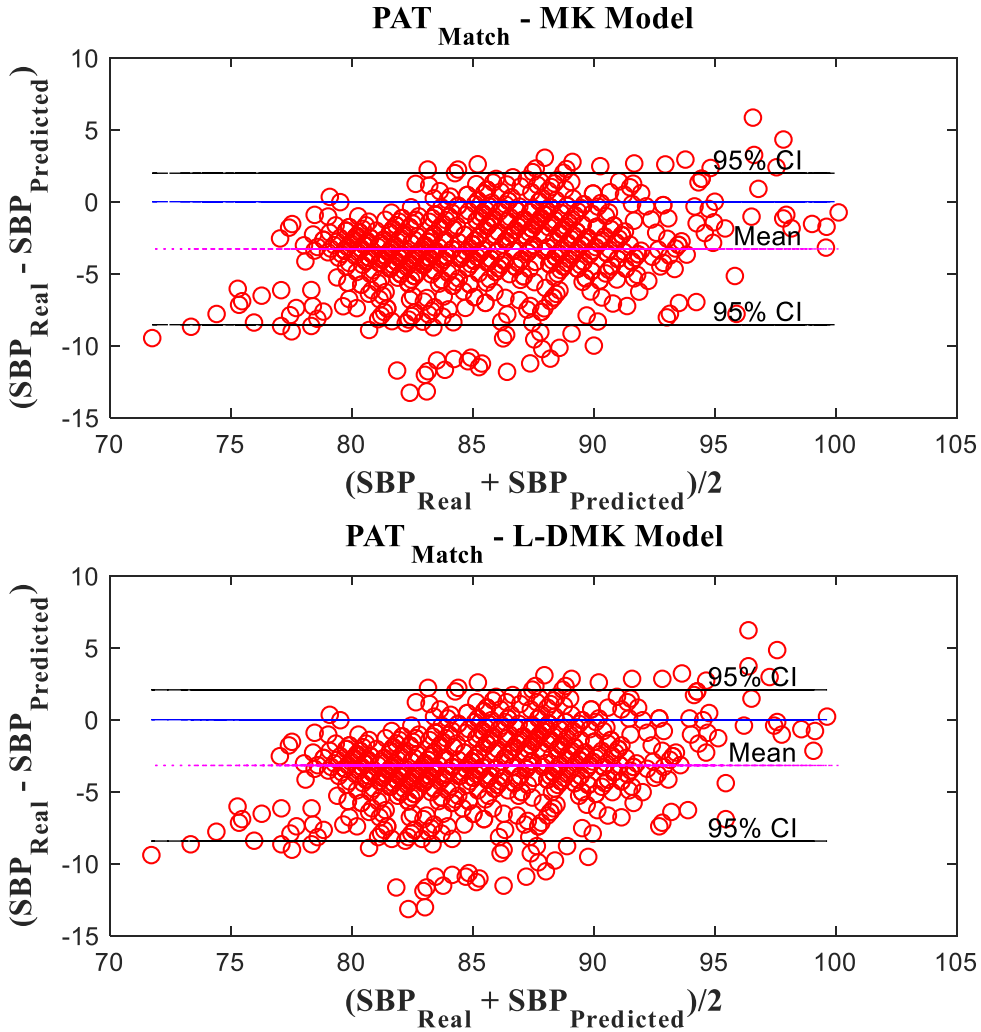

Fig.5.3. Bland-Altman plot showing agreement difference between real SBP and predicted SBP for PAT_{Match} which was created by MK model and L-DMK model for volunteer 4.

The calculated 95% confidence range is between -8.5483 mmHg and 1.9789 mmHg which are lower confidence interval and upper confidence interval respectively for MK model and between 2.0734 mmHg and -8.4348 mmHg for L-DMK model. The standard deviation difference is calculated as

2.6855 mmHg for MK-model and 2.6807 mmHg for L-DMK model. According to the Association for the Advancement of Medical Instrumentation (AAMI) in the United States, the mean difference which is less than 5mmHg and difference in standard deviation not exceeding 8 mmHg were good results [51]. Hence, the result from volunteer 4 for PAT_{Match} on Fig. 5.3 is a good result. Both models have not shown any changes in mean difference and standard deviation difference even though they are linear and non-linear models.

Secondly, models were created on rest session 2 and tested on rest session 4 for SBP and the correlation of models with PAT values is calculated. Even though volunteer 2 and 3 has weak and very weak correlation, volunteer 1 has moderate uphill correlation such as $r = 0.4635$ and $r = 0.4621$ for PAT_{Match}, $r = 0.4878$ and $r = 0.4867$ for $PAT_{Slope50}$ and $r = 0.4453$ and $r = 0.4448$ for PAT_{SSF} when tested on MK and L-DMK model respectively. The correlation of real SBP and predicted SBP for volunteer 4 is found to be $r = 0.8643$ and $r = 0.8659$ for PAT_{Match}, $r = 0.8655$ and $r = 0.8672$ for $PAT_{Slope50}$ and $r = 0.8688$ and $r = 0.8701$ for PAT_{SSF} when tested on MK and L-DMK model respectively.

Table 7. Models created on rest session 2 for SBP and tested on rest session 4 and their real and predicted SBP correlation with PAT methods.

Volunteer	**MK Model**			**L-DMK Model**		
	PAT_{Match} (*r* values)	**$PAT_{Slope50}$ (*r* values)**	**PAT_{SSF} (*r* values)**	**PAT_{Match} (*r* values)**	**$PAT_{Slope50}$ (*r* values)**	**PAT_{SSF} (*r* values)**
1	0.4635	0.4878	0.4453	0.4621	0.4867	0.4448
2	-0.1908	-0.1990	-0.1812	-0.1870	-0.1957	-0.1793
3	-0.0485	-0.1291	0.0391	-0.0638	-0.1424	0.0298
4	0.8643	0.8655	0.8688	0.8659	0.8672	0.8701

The results were checked using the agreements (see Fig. 5.4) which is tested for volunteer 4 for PAT_{SSF} created by the MK model and L-DMK model. The correlation coefficient of the volunteer 4 for PAT_{SSF} when created by MK model is found to be $r = 0.8688$ and for L-DMK model is found to be $r = 0.8701$ as illustrated in Table 7. MK model has the mean difference as -4.6711 mmHg with 95% confidence range between -0.7865 and -8.5556 and their difference in standard deviation is 1.9891 mmHg. The mean difference of L-DMK model is -4.4420 mmHg with the 95% confidence range as -0.6554 for upper confidence interval and -8.2285 for lower confidence interval with standard deviation difference as 1.9319 mmHg. As per the validation protocol by AAMI, the mean difference and standard deviation difference of both models were good, and they are similar.

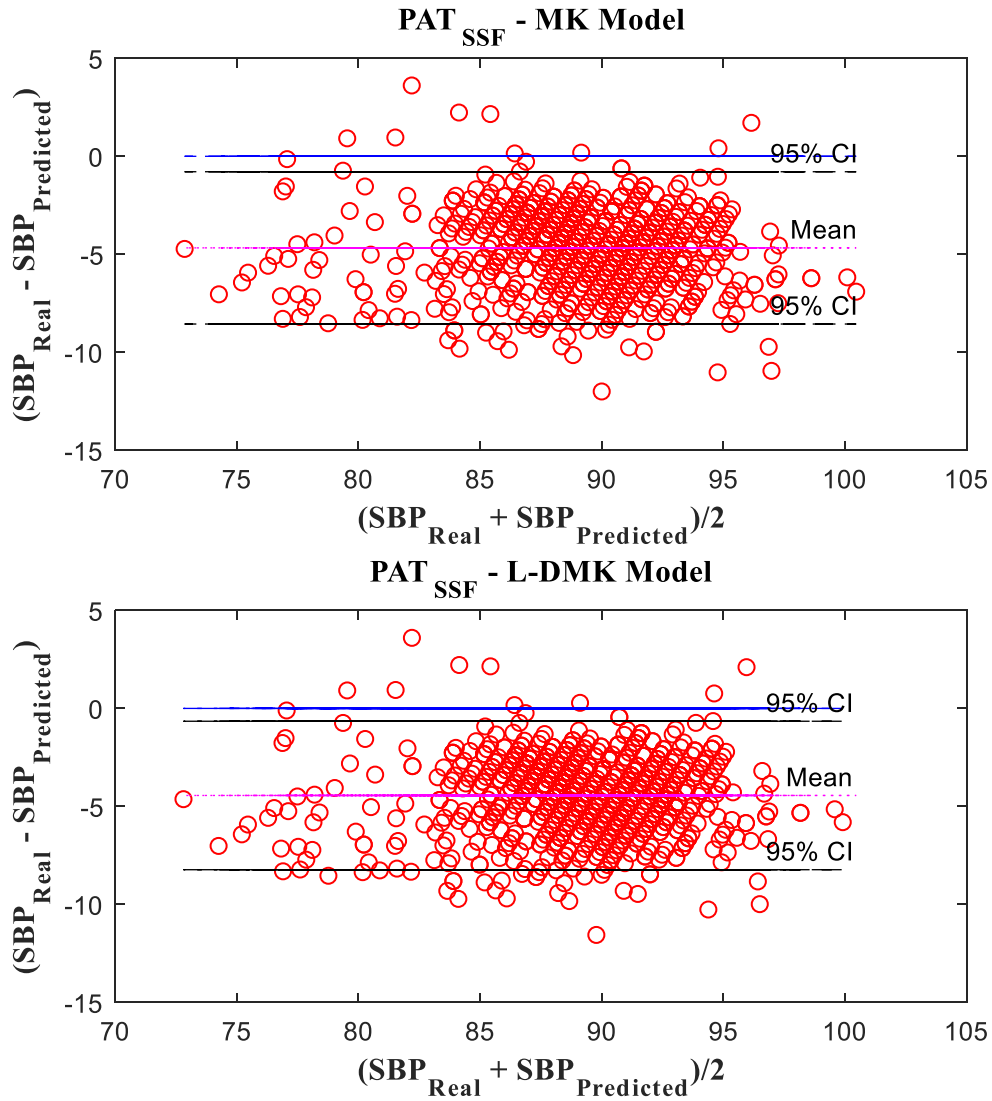

Fig. 5.4. Bland-Altman plot showing agreement difference between real SBP and predicted SBP for PAT_{SSF} which was created by L-DMK model for volunteer 4.

When the model, created on rest session 2 is tested on rest session 5 to calculate real SBP and predict SBP, the correlation coefficient for MK model and L-DMK model is found to be strong uphill correlation $r = 0.7005$ and $r = 0.6976$ for PAT_{Match}, $r = 0.7021$ and $r = 0.6979$ for $PAT_{Slope50}$ and $r = 0.6619$ and $r = 0.6605$ for PAT_{SSF} for volunteer 1 while volunteer 3 and 4 has weak and very weak correlation respectively. Volunteer 2 has downhill moderate correlation for PAT_{Match} as $r = -0.3915$ and $r = -0.4050$ for $PAT_{Slope50}$ when created using MK model and $r = -0.3969$ for $PAT_{Slope50}$ when created using L-DMK model.

Table 8. Models created on rest session 2 for SBP and tested on rest session 5 and their real and predicted SBP correlation with PAT methods.

Volunteer	MK Model			L-DMK Model		
	PAT_{Match} (*r* values)	$PAT_{Slope50}$ (*r* values)	PAT_{SSF} (*r* values)	PAT_{Match} (*r* values)	$PAT_{Slope50}$ (*r* values)	PAT_{SSF} (*r* values)
1	0.7005	0.7021	0.6619	0.6976	0.6979	0.6605
2	-0.3915	-0.4050	-0.3733	-0.3842	-0.3969	-0.3673
3	-0.3798	-0.3844	-0.3570	-0.3781	-0.3832	-0.3562
4	0.0369	0.0392	0.0800	0.0351	0.0371	0.0775

The volunteer 1 result is checked by the scatter plot showing the real and predicted SBP for $PAT_{Slope50}$ while created by MK model and L-DMK model (see Fig. 5.5).

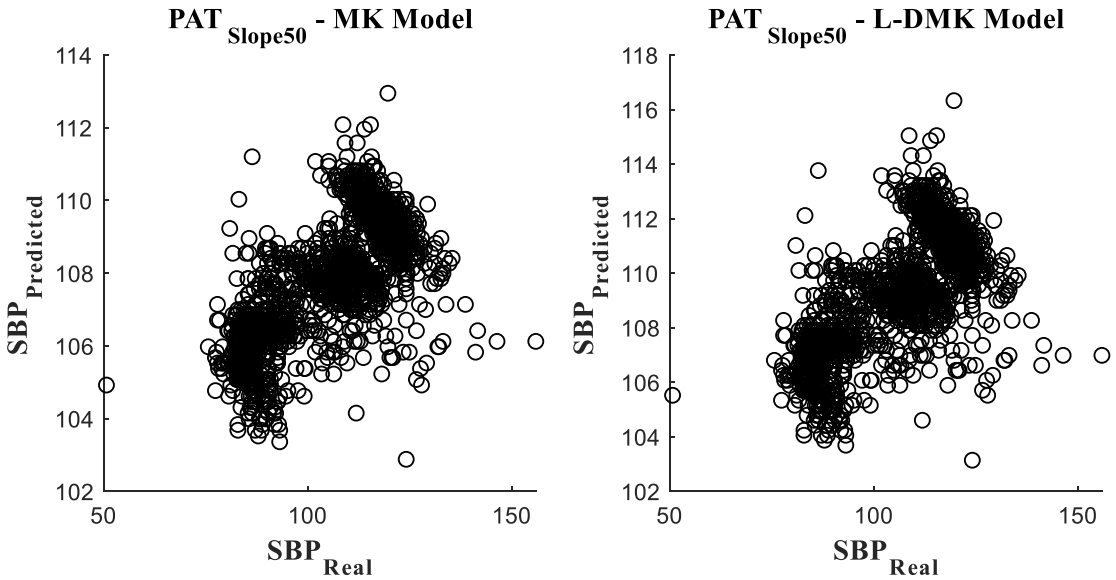

Fig. 5.5. Scattered plot for real SBP and Predicted SBP for volunteer 1, MK model (left) and L-DMK model (right) for $PAT_{Slope50}$.

The models did not show any difference for any volunteers and for any PAT methods and hence their correlation is quite similar. When the rest session 2 is used for creating the models and tested on rest session 3 to 5, initially the correlation has increased from rest session 3 to 4 for all volunteers except volunteer 3. But the rest session 5 has sudden drop in correlation for volunteer 4 comparted to other volunteers. This change would have occurred due to the synchronization problems of Portapres and Nautilus and hence which resulted in quite low correlation.

5.2. Estimated PAT values and models for breathing test database

The PAT values of breathing test for three estimated methods were calculated. It is observed that the PAT values are similar for all methods (see Fig.5.6). PAT_{Match} and $PAT_{slope50}$ has the variations from 250 ms to 210 ms while PAT_{SSF} has the variations from 350 ms to 260 ms.

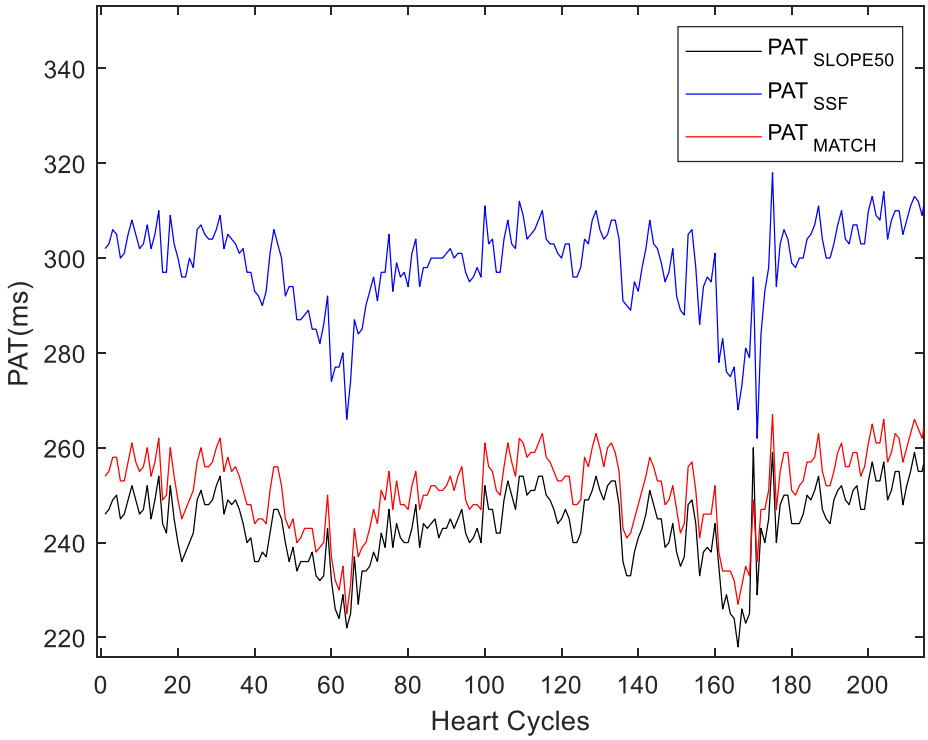

Fig. 5.6. PAT for three different methods for breathing test database for volunteer no.5.

The Pearson correlation coefficients of BP parameters with PAT values were calculated for breathing test for all volunteers and illustrated in Table 11.

Table 9. Correlation coefficients of BP parameters and PAT methods for breathing test

Volunteer	**PAT_{Match} (*r* values)**				**$PAT_{Slope50}$ (*r* values)**				**PAT_{SSF} (*r* values)**			
	SBP	**MBP**	**DBP**	**PP**	**SBP**	**MBP**	**DBP**	**PP**	**SBP**	**MBP**	**DBP**	**PP**
1	-0.5586	-0.5209	-0.4222	-0.4261	-0.5206	-0.4538	-0.3401	-0.4438	-0.5684	-0.5664	-0.4908	-0.3800
2	-0.6512	-0.5421	-0.3862	-0.6919	-0.5713	-0.4652	-0.3193	-0.6225	-0.6650	-0.5628	-0.4115	-0.6929
3	-0.4829	-0.3232	-0.1120	-0.6385	-0.4816	-0.3198	-0.1066	-0.6402	-0.4997	-0.3421	-0.1317	-0.6505
4	-0.5257	-0.4676	-0.3443	-0.5088	-0.4763	-0.4185	-0.3021	-0.4674	-0.4846	-0.4293	-0.3140	-0.4713
5	-0.6849	-0.6075	-0.4417	-0.5296	-0.6686	-0.5873	-0.4218	-0.5246	-0.6725	-0.5997	-0.4389	-0.5160

From the Table 9, we can say that SBP is having highest correlation with all PAT methods i.e. strong downhill correlation with PAT_{Match} for volunteer 2 as $r = -0.6512$ and for volunteer 5 as $r = -0.6849$, with $PAT_{Slope50}$ for volunteer 5 as $r = -0.6686$ and finally with PAT_{SSF} for volunteer 2 as $r = -0.6650$ and for volunteer 5 as $r = -0.6725$. Then PP shows strong downhill correlation with PAT_{Match} calculated as $r = -0.6919$ and $r = -0.6385$, with $PAT_{Slope50}$ is calculated as $r = -0.6225$ and $r = -0.6402$, with PAT_{SSF} is estimated as $r = -0.6929$ and $r = -0.6505$ for volunteers 2 and 3 respectively. MBP has the strong downhill correlation only for volunteer 5 such that $r = -0.6075$ and $r = -0.5997$ with PAT_{Match} and PAT_{SSF} respectively. The other volunteers have moderate downhill correlation and few with weak correlation but only DBP is having very weak correlation for volunteer 3 i.e. $r = -0.1120$, $r = -0.1066$ and $r = -0.1317$ with PAT_{Match}, $PAT_{Slope50}$ and PAT_{SSF} respectively. The correlation for volunteer 5 is shown as scatter plot which proves that SBP and MBP has the strong downhill correlation while DBP and PP has the moderate downhill correlation (see Fig 5.7). It is

observed that SBP and PP were having downhill moderate and downhill strong correlation while MBP has downhill moderate, weak and strong correlation. But DBP is the only parameter which do not have strong correlation despite of moderate, weak and very weak correlation. PAT_{Match} and PAT_{SSF} methods have shown similar correlation while PAT_{SSF} have shown quite low correlation.

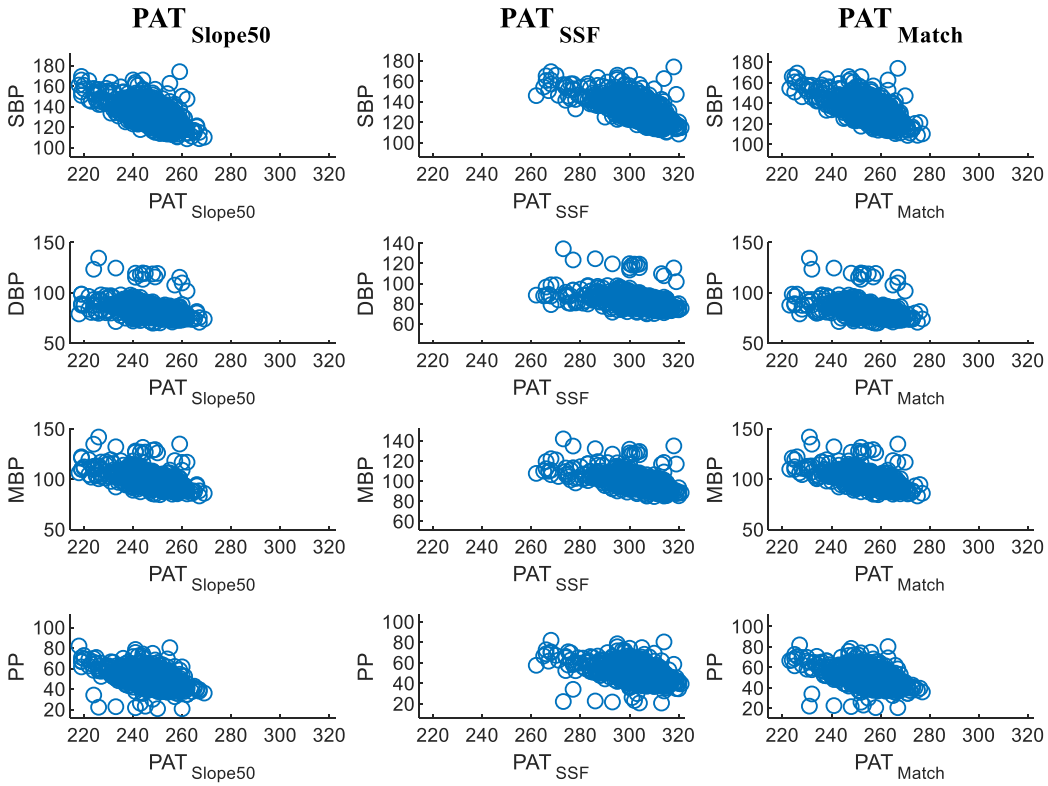

Fig. 5.7. Scatter plot showing correlation between BP parameters and three PAT methods for breathing test, volunteer no.5.

Breathing test database is divided into two sessions: Valsalva manoeuvre and full controlled respiration so that the models can be created for Valsalva manoeuvre session and tested on full controlled respiration session. In order to test the selected models, Valsalva manoeuvre session is used for creating the model which provides real SBP and it is tested on full controlled respiration session which provides predicted SBP. The Pearson correlation coefficient *r* of real and predicted SBP created and tested by MK and L-DMK model for PAT_{Match}, $PAT_{Slope50}$ and PAT_{SSF} is shown in Table 10.

Table 10. Models created on Valsalva manoeuvre session for SBP and tested on full controlled respiration session and their real and predicted SBP correlation with PAT methods.

Volunteer	**MK Model**			**L-DMK Model**		
	PAT_{Match} (*r* values)	**$PAT_{Slope50}$ (*r* values)**	**PAT_{SSF} (*r* values)**	**PAT_{Match} (*r* values)**	**$PAT_{Slope50}$ (*r* values)**	**PAT_{SSF} (*r* values)**
1	0.4447	0.4529	0.4313	0.4392	0.4473	0.4271
2	0.6083	0.5770	0.6578	0.6071	0.5754	0.6568
3	0.5872	0.5995	0.5848	0.5853	0.5963	0.5830
4	0.4614	0.4265	0.4301	0.4589	0.4251	0.4283
5	0.6456	0.6325	0.6474	0.6429	0.6296	0.6450

The Table 10 clearly shows that all the volunteers have either strong uphill correlation or moderate correlation which is quite a good result. Volunteer 2 and volunteer 5 has strong uphill correlation for PAT_{Match} when created by MK model such that Pearson correlation coefficient, *r = 0.6083* and *r = 0.6456*, for PAT_{SSF} as *r = 0.6578* and *r = 0.6474* respectively. Volunteer 3 and volunteer 5 has strong uphill correlation for $PAT_{Slope50}$ with the MK model provided the coefficients as *r = 0.5995* and *r = 0.6325* respectively. When the L-DMK model is used, the correlation of real and predicted SBP for PAT_{Match} is given as *r = 0.6071* and *r = 0.6429*, for PAT_{SSF} is given as *r = 0.6568* and *r = 0.6450* for volunteer 2 and volunteer 5 respectively. Likewise, for $PAT_{Slope50}$, the correlation is *r = 0.5963* and *r = 0.6296* for volunteer 3 and volunteer 5 respectively. It is observed that both models have uphill strong and moderate correlation with all PAT methods.

Bland-Altman plot is plotted to see the difference of agreements between SBP real and SBP predicted which was created by MK model and L-DMK model for PAT_{Match} on Valsalva manoeuvre session and full controlled respiration session for predicting (see Fig. 5.8) for volunteer 5. The mean difference is -4.0917 mmHg and their Pearson correlation coefficient are *r = 0.6456* which is a strong uphill correlation for MK model as illustrated in Table 10.

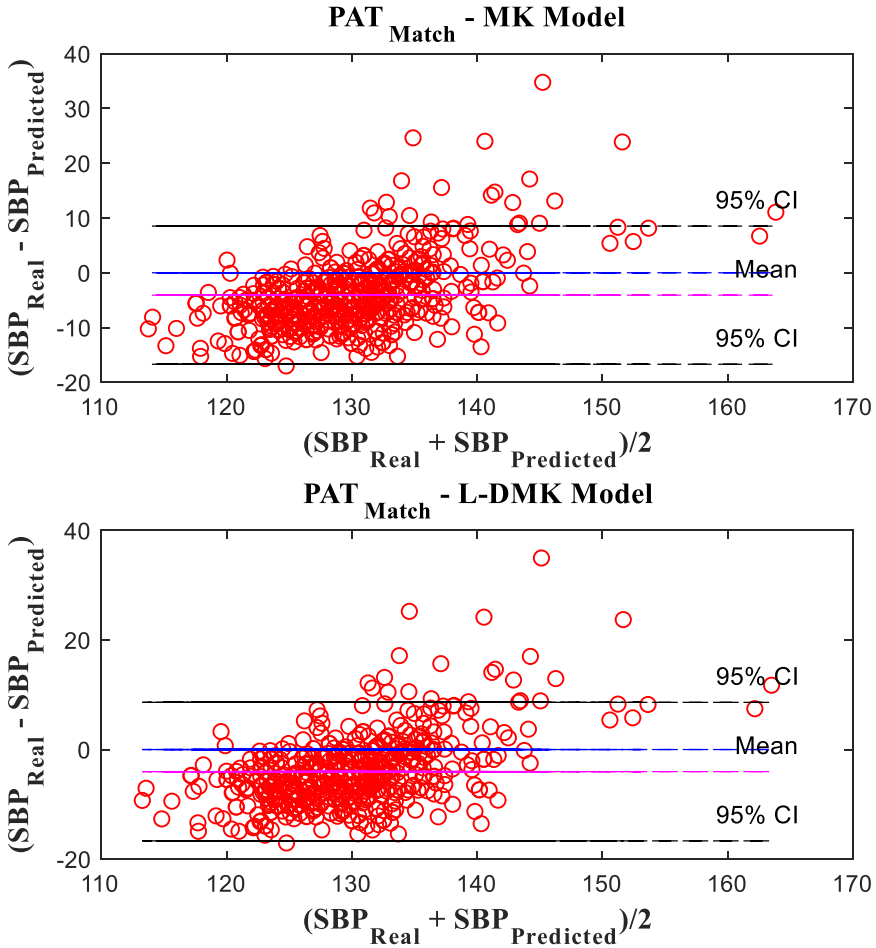

Fig. 5.8. Bland-Altman plot showing agreement difference between real SBP and predicted SBP for PAT_{Match} which was created by MK model and L-DMK for volunteer 5.

For MK model, the 95% confidence range is estimated as 8.5209 mmHg and -16.7044 mmHg for upper and lower confidence interval respectively with difference in standard deviation as 6.4350 mmHg. The mean difference for L-DMK model is -4.0323 mmHg with 95% confidence range

between 8.6141 mmHg and -16.6787 mmHg and their standard deviation difference is 6.4522 mmHg. It is observed that this result is quite good as per AAMI's validation protocol.

When the MK model and L-DMK model is used, PAT_{SSF} for volunteer 5 is illustrated in Bland-Altman plot (see Fig. 5.9).

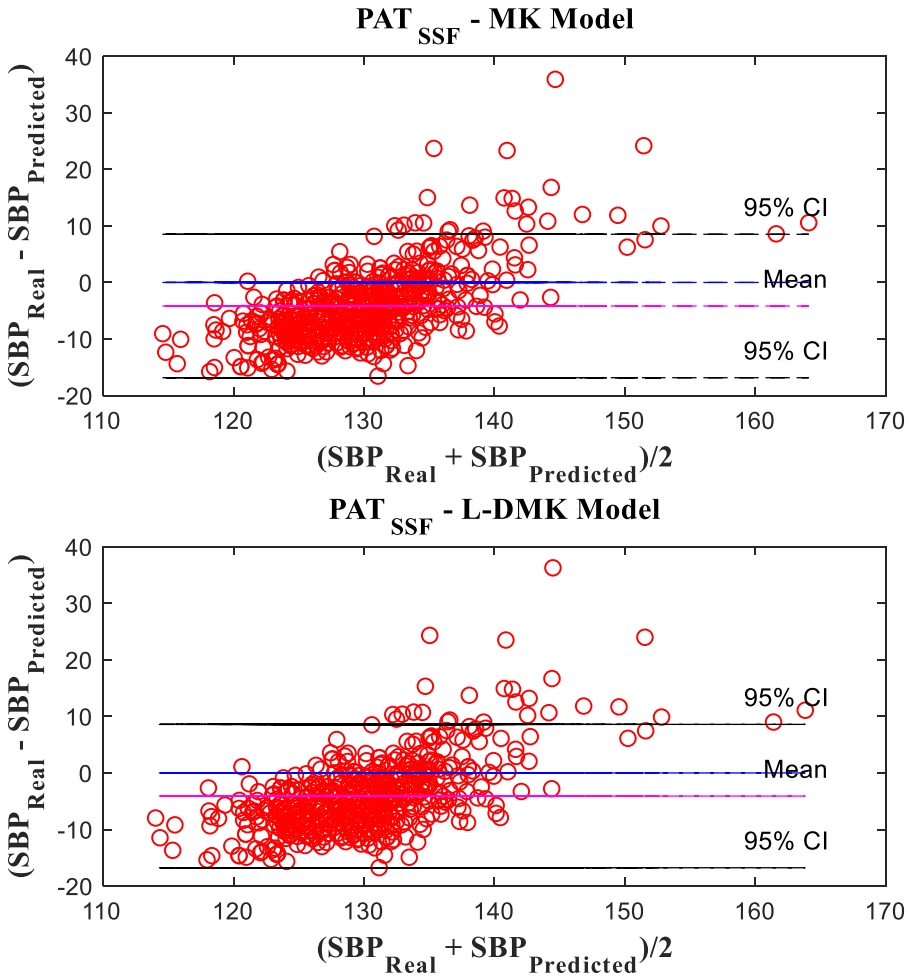

Fig. 5.9 Bland-Altman plot showing agreement difference between real SBP and predicted SBP for PAT_{SSF} which was created by MK model and L-DMK model for volunteer 5.

The MK model with PAT_{SSF} has the mean difference as -4.1669 mmHg with standard deviation as 6.4722 mmHg. The 95% confidence range is calculated for MK model which is between the range 8.5186 mmHg and -16.8523 mmHg. Similarly, for the L-DMK model, mean difference is -4.0878 mmHg and their Pearson correlation coefficient are $r = 0.6450$ which is a strong uphill correlation as illustrated in Table 10. The 95% confidence range is estimated as 8.5877 mmHg and -16.7634 mmHg for upper and lower confidence interval respectively with difference in standard deviation as 6.4671 mmHg. From this result it is observed that both models are similar in mean difference and standard deviation deviation and it is good as per validation protocol of AAMI.

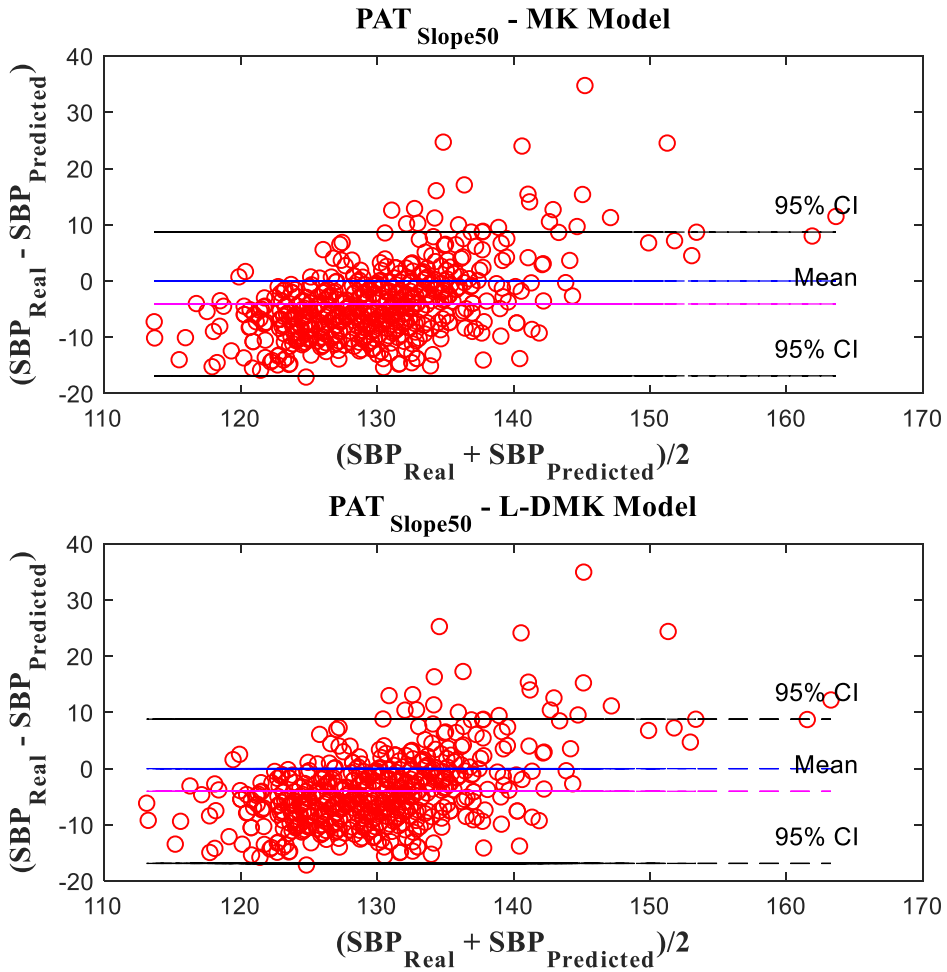

Fig 5.10. Bland-Altman plot showing agreement difference between real SBP and predicted SBP for $PAT_{Slope50}$ which was created by MK model and L-DMK model for volunteer 5.

Bland-Altman plot is plotted for MK model and L-DMK model for $PAT_{Slope50}$ which has the mean difference as -4.0855 mmHg and -4.0282 mmHg respectively. The 95% confidence range for MK model is calculated as in the range between 8.7033 mmHg and -16.7042 mmHg while for L-DMK model the range is between 8.8032 mmHg and -16.8596 mmHg. The difference in standard deviation is 6.5249 mmHg for MK model and 6.5467 mmHg for L-DMK model. The Fig.5.10 shows that the mean is increasing from down to top. The results were similar in despite of different models and different PAT methods and the results were quite good according to AAMI's validation protocol.

All PAT methods have shown good correlation with two models and the results were similar nevertheless the linear or non-linear model.

Conclusions

1. Hypertensive patients with non-dipping nocturnal blood pressure and morning surge are at higher risk of cardiovascular diseases and their blood pressure parameters should be monitored unobtrusively for a long-term. A scientific literature review of methods for long-term blood pressure monitoring showed that methods based on pulse arrival time estimation from synchronously recorded electrocardiogram and photoplethysmogram could be an attractive continuous, non-invasive and unobtrusive solution to this problem.
2. Three different algorithms for fiducial point detection in photoplethysmogram pulse wave were implemented and used for pulse arrival time estimation. The selected fiducial point definitions are middle amplitude of pulse slope, peak of slope sum function and peak of matched filtered photoplethysmogram.
3. Implemented algorithms were tested on signals from two databases. Thermal stress and breathing tests (Valsalva maneuver and full controlled respiration) were used in these databases to induce changes in blood pressure parameters. However, moderate to strong correlation between pulse arrival time values and reference blood pressure values was obtained using breathing test database only. Possible shortcomings when using thermal stress database could be insufficient change in blood pressure due to thermal stress or synchronization problems between the device, used for recording reference blood pressure signal, and the device, used for electrocardiogram and photoplethysmogram acquisition.
4. The results obtained on breathing test database showed that pulse arrival time are moderately or strongly correlated with systolic blood pressure, mean blood pressure and pulse pressure. However, pulse arrival time is weakly correlated with diastolic blood pressure, especially when using middle amplitude of pulse slope to obtain the fiducial point of the pulse wave. When blood pressure estimation models based on pulse arrival time, namely Moens-Korteweg exponential arterial elasticity model and derivative of Moens-Korteweg linear model, were created and tested, the correlation of real and predicted systolic blood pressure values was found to be moderate (0.4–0.59) or strong (0.6–0.79) similarly for both models. Moreover, mean difference between real and predicted systolic blood pressure values was <5 mmHg and standard deviation of difference was <8 mmHg showing good agreement for both models. Hence, both blood pressure estimation models are working similarly independently of their complexity.

List of References

1. ECOBICI, Monica and STOICESCU, Claudiu. Arterial Stiffness and Hypertension - Which Comes First? *Maedica* [online]. 2017. Vol. 12, no. 3, p. 184–190.
2. JONES, Daniel W., HALL, John E., ROCCELLA, Edward J., FALKNER, Bonita E., KURTZ, Theodore, SHEPS, Sheldon G., GRAVES, John, PICKERING, Thomas G., APPEL, Lawrence J. and HILL, Martha N. Recommendations for Blood Pressure Measurement in Humans and Experimental Animals. *Hypertension*. 2004. Vol. 45, no. 1, p. 142–161. Available from: doi:10.1161/01.hyp.0000150859.47929.8e.
3. AL-ZABEN, Awad, FORA, Malak and OBAIDAT, Aseel. Detection of premature ventricular beats from arterial blood pressure signal. *Middle East Conference on Biomedical Engineering, MECBME*. 2018. Vol. 2018-March, p. 17–19. Available from: doi:10.1109/MECBME.2018.8402398.
4. PALANIAPPAN, R. and KRISHNAN, S.M. Detection of ectopic heart beats using ECG and blood pressure signals. . 2005. No. 1, p. 573–576. Available from: doi:10.1109/spcom.2004.1458525.
5. KARIO, Kazuomi. Morning Surge in Blood Pressure and Cardiovascular Risk. *Hypertension*. 2010. Vol. 56, no. 5, p. 765–773. Available from: doi:10.1161/hypertensionaha.110.157149.
6. YANO, Yuichiro and KARIO, Kazuomi. Nocturnal blood pressure, morning blood pressure surge, and cerebrovascular events. *Current Hypertension Reports*. 2012. Vol. 14, no. 3, p. 219–227. Available from: doi:10.1007/s11906-012-0261-z.
7. PIERDOMENICO, Sante D., PIERDOMENICO, Anna M. and CUCCURULLO, Franco. Morning blood pressure surge, dipping, and risk of ischemic stroke in elderly patients treated for hypertension. *American Journal of Hypertension*. 2014. Vol. 27, no. 4, p. 564–570. Available from: doi:10.1093/ajh/hpt170.
8. PIERDOMENICO, Sante D., PIERDOMENICO, Anna M., DI TOMMASO, Roberta, COCCINA, Francesca, DI CARLO, Silvio, PORRECA, Ettore and CUCCURULLO, Franco. Morning blood pressure surge, dipping, and risk of coronary events in elderly treated hypertensive patients. *American Journal of Hypertension*. 2016. Vol. 29, no. 1, p. 39–45. Available from: doi:10.1093/ajh/hpv074.
9. CHUNG, Elena, CHEN, Guo, ALEXANDER, Brenton and CANNESSON, Maxime. Non-invasive continuous blood pressure monitoring: A review of current applications. *Frontiers of Medicine in China*. 2013. Vol. 7, no. 1, p. 91–101. Available from: doi:10.1007/s11684-013-0239-5.
10. RAJALA, Satu, AHMANIEMI, Teemu, LINDHOLM, Harri and TAIPALUS, Tapio. Pulse arrival time (PAT) measurement based on arm ECG and finger PPG signals - Comparison of PPG feature detection methods for PAT calculation. *Proceedings of the Annual International Conference of the IEEE Engineering in Medicine and Biology Society, EMBS*. 2017. P. 250–253. Available from: doi:10.1109/EMBC.2017.8036809.
11. JANG, Dae-Geun, PARK, Sangjun, HAHN, Minsoo and PARK, Seung-Hun. A Real-Time Pulse Peak Detection Algorithm for the Photoplethysmogram. *International Journal of Electronics and Electrical Engineering*. 2014. Vol. 2, no. 1, p. 45–49. Available from: doi:10.12720/ijeee.2.1.45-49.
12. PALIAKAITĖ, Birutė, DAUKANTAS, Saulius and MAROZAS, Vaidotas. Assessment of pulse arrival time for arterial stiffness monitoring on body composition scales. *Computers in Biology and Medicine*. 2017. Vol. 85, p. 135–142. Available from: doi:10.1016/j.compbiomed.2016.04.012.
13. PERALTA, Elena, LAZARO, Jesus, BAILON, Raquel, MAROZAS, Vaidotas and GIL, Eduardo. Optimal fiducial points for pulse rate variability analysis from forehead and finger photoplethysmographic signals. *Physiological Measurement* [online]. 26 February 2019.

Vol. 40, no. 2, p. 025007. [Accessed 16 May 2019]. Available from: doi:10.1088/1361-6579/ab009b.

14. CHANWIMALUEANG, Theerasak, VON ROSENBERG, Wilhelm and MANDIC, Danilo P. Enabling R-peak detection in wearable ECG: Combining matched filtering and Hilbert transform. *International Conference on Digital Signal Processing, DSP*. 2015. Vol. 2015-Septe, p. 134–138. Available from: doi:10.1109/ICDSP.2015.7251845.
15. ZURICH, E T H, SOL, Josep Maria, CH, Olivier and LOELIGER, Andrea. Continuous non - invasive blood pressure estimation. . 2011. No. 20093.
16. Cardiovascular System - Human Veins, Arteries, Heart. [online]. [Accessed 26 February 2019].
17. POLLOCK, Joshua D. and MAKARYUS, Amgad N. *Physiology, Cardiac Cycle* [online]. StatPearls Publishing, 2019. [Accessed 20 March 2019].
18. KUNDU, Ramendra, BISWAS, Subir and DAS, Mithun. Mean Arterial Pressure Classification: A Better Tool for Statistical Interpretation of Blood Pressure Related Risk Covariates. *Cardiology and Angiology: An International Journal* [online]. 10 January 2017. Vol. 6, no. 1, p. 1–7. [Accessed 20 March 2019]. Available from: doi:10.9734/CA/2017/30255.
19. BRADSHAW, Wendi. The importance of mean arterial pressure as a patient assessment tool: in haemodialysis and acute care. *Australian nursing journal* [online]. 2012. Vol. 20, no. 2, p. 26–29.
20. HOMAN, Travis D. and CICHOWSKI, Erica. *Physiology, Pulse Pressure* [online]. StatPearls Publishing, 2019. [Accessed 24 March 2019].
21. KAWANO, Yuhei. Diurnal blood pressure variation and related behavioral factors. *Hypertension Research* [online]. 2011. Vol. 34, no. 3, p. 281–285. Available from: doi:10.1038/hr.2010.241.
22. COCCINA, Francesca, LAPENNA, Domenico, PIERDOMENICO, Anna M., PORRECA, Ettore and PIERDOMENICO, Sante D. Prognostic Value of Nondipping and Morning Surge in Elderly Treated Hypertensive Patients With Controlled Ambulatory Blood Pressure. *American Journal of Hypertension*. 2016. Vol. 30, no. 2, p. 159–165. Available from: doi:10.1093/ajh/hpw145.
23. BILO, Grzegorz, GRILLO, Andrea, GUIDA, Valentina and PARATI, Gianfranco. Morning blood pressure surge: pathophysiology, clinical relevance and therapeutic aspects. *Integrated Blood Pressure Control*. 2018. Vol. Volume 11, p. 47–56. Available from: doi:10.2147/ibpc.s130277.
24. KIM, Min Woong, KIM, Bum Soo, SHIN, Hun Sub, KIM, Byung Jin, SUNG, Ki Chul, KANG, Jin Ho, LEE, Man Ho, PARK, Jung Ro, KIM, Hwa Mock and KIM, Heung Dae. Lack of Correlation Between QTc Dispersion and Morning Blood Pressure Surge in Recently Diagnosed Essential Hypertensive Patients. *Circulation Journal*. 2007. Vol. 71, no. 8, p. 1288–1292. Available from: doi:10.1253/circj.71.1288.
25. ALLEN, John. Photoplethysmography and its application in clinical physiological measurement. *Physiological measurement* [online]. 2007. Vol. 28, no. 3, p. R1-39. Available from: doi:10.1088/0967-3334/28/3/R01.
26. WANG, Guoxing, ATEF, Mohamed and LIAN, Yong. Towards a Continuous Non-Invasive Cuffless Blood Pressure Monitoring System Using PPG: Systems and Circuits Review. *IEEE Circuits and Systems Magazine*. 2018. Vol. 18, no. 3, p. 6–26. Available from: doi:10.1109/MCAS.2018.2849261.
27. ELGENDI, Mohamed, FLETCHER, Rich, NORTON, Ian, BREARLEY, Matt, ABBOTT, Derek, LOVELL, Nigel H. and SCHUURMANS, Dale. On time domain analysis of photoplethysmogram signals for monitoring heat stress. *Sensors (Switzerland)*. 2015. Vol. 15,

no. 10, p. 24716–24734. Available from: doi:10.3390/s151024716.

28. MCDUFF, Daniel, GONTAREK, Sarah and PICARD, Rosalind W. *Remote Detection of Photoplethysmographic Systolic and Diastolic Peaks Using a Digital Camera* [online]. 2013. [Accessed 7 April 2019].
29. TARVIRDIZADEH, Bahram, GOLGOUNEH, Alireza, KHODABAKHSHI, Erfan and TAJDARI, Farzam. An assessment of a similarity between the right and left hand Photoplethysmography signals, using time and frequency features of heart-rate-variability signal. In : *2017 IEEE 4th International Conference on Knowledge-Based Engineering and Innovation (KBEI)* [online]. IEEE, December 2017. p. 0588–0594. [Accessed 7 April 2019]. ISBN 978-1-5386-2640-5.
30. BECKER, Daniel E. Fundamentals of electrocardiography interpretation. *Anesthesia progress* [online]. 2006. Vol. 53, no. 2, p. 53–63; quiz 64. [Accessed 21 April 2019]. Available from: doi:10.2344/0003-3006(2006)53[53:FOEI]2.0.CO;2.
31. ASHLEY, Euan A and NIEBAUER, Josef. Conquering the ECG. [online]. 2004. [Accessed 21 April 2019].
32. ECG Basics • LITFL Medical Blog • LITFL ECG Library. [online]. [Accessed 7 April 2019].
33. MHRA. Blood Pressure Measurement Devices. [online]. 2013. Vol. 2, no. 1, p. 1–16.
34. CENTRAL, Follow Biomed. Oscillometric measurement of systolic and diastolic blood pressures validated in a physiologic mathematical model. . 2016. P. 1–31. Available from: doi:10.1186/1475-925X-11-56.
35. FORTIN, J., MARTE, W., GRÜLLENBERGER, R., HACKER, A., HABENBACHER, W., HELLER, A., WAGNER, CH, WACH, P. and SKRABAL, F. Continuous non-invasive blood pressure monitoring using concentrically interlocking control loops. *Computers in Biology and Medicine*. 2006. Vol. 36, no. 9, p. 941–957. Available from: doi:10.1016/j.compbiomed.2005.04.003.
36. LEE, Jeon and CHANG, Ki. Tonometric Vascular Function Assessment. In : *Biomedical Engineering* [online]. InTech, 2009. [Accessed 7 April 2019].
37. Finapres Medical Systems |. [online]. [Accessed 7 April 2019].
38. SHARMA, Manuja, BARBOSA, Karinne, HO, Victor, GRIGGS, Devon, GHIRMAI, Tadesse, KRISHNAN, Sandeep, HSIAI, Tzung, CHIAO, Jung-Chih and CAO, Hung. Cuff-Less and Continuous Blood Pressure Monitoring: A Methodological Review. *Technologies* [online]. 2017. Vol. 5, no. 2, p. 21. Available from: doi:10.3390/technologies5020021.
39. SALVI, Paolo. *Pulse Waves*. 2012. ISBN 978-88-470-2438-0.
40. HAHN, Jin-Oh, MESTHA, Lalit K., MUKKAMALA, Ramakrishna, KIM, Chang-Sei, INAN, Omer T., TOREYIN, Hakan and KYAL, Survi. Toward Ubiquitous Blood Pressure Monitoring via Pulse Transit Time: Theory and Practice. *IEEE Transactions on Biomedical Engineering*. 2015. Vol. 62, no. 8, p. 1879–1901. Available from: doi:10.1109/tbme.2015.2441951.
41. PIELMUŞ, Alexandru-Gabriel, PFLUGRADT, Maik, TIGGES, Timo, KLUM, Michael, FELDHEISER, Aarne, HUNSICKER, Oliver and ORGLMEISTER, Reinhold. Novel computation of pulse transit time from multi-channel PPG signals by wavelet transform. *Current Directions in Biomedical Engineering*. 2016. Vol. 2, no. 1, p. 209–213. Available from: doi:10.1515/cdbme-2016-0047.
42. LI, Yanjun, WANG, Zengli, ZHANG, Lin, YANG, Xianglin and SONG, Jinzhong. Characters available in photoplethysmogram for blood pressure estimation: Beyond the pulse transit time. *Australasian Physical and Engineering Sciences in Medicine*. 2014. Vol. 37, no. 2, p. 367–376. Available from: doi:10.1007/s13246-014-0269-6.
43. LIN, Chen, ZHOU, Yuan, WANG, Hu and WANG, Yao. Pulse waveform as an indicator of baseline offset in pulse transit time based blood pressure estimation. *2017 IEEE Healthcare*

Innovations and Point of Care Technologies, HI-POCT 2017. 2017. Vol. 2017-Decem, p. 26–31. Available from: doi:10.1109/HIC.2017.8227576.

44. LIN, Wan Hua, WANG, Hui, SAMUEL, Oluwarotimi Williams and LI, Guanglin. Using a new PPG indicator to increase the accuracy of PTT-based continuous cuffless blood pressure estimation. *Proceedings of the Annual International Conference of the IEEE Engineering in Medicine and Biology Society, EMBS*. 2017. P. 738–741. Available from: doi:10.1109/EMBC.2017.8036930.
45. HEMON, Mathilde C. and PHILLIPS, Justin P. Comparison of foot finding methods for deriving instantaneous pulse rates from photoplethysmographic signals. *Journal of Clinical Monitoring and Computing*. 2016. Vol. 30, no. 2, p. 157–168. Available from: doi:10.1007/s10877-015-9695-6.
46. BAEK, Hyun Jae, KIM, Jung Soo, KIM, Yun Sung, LEE, Haet Bit and PARK, Kwang Suk. Second derivative of photoplethysmography for estimating vascular aging. *Proceedings of the IEEE/EMBS Region 8 International Conference on Information Technology Applications in Biomedicine, ITAB*. 2008. Vol. 00, p. 70–72. Available from: doi:10.1109/ITAB.2007.4407346.
47. ELGENDI, Mohamed. On the analysis of fingertip photoplethysmogram signals. *Current cardiology reviews* [online]. February 2012. Vol. 8, no. 1, p. 14–25. [Accessed 23 April 2019]. Available from: doi:10.2174/157340312801215782.
48. RAPALIS, Andrius. *Kaunas University of Technology Physiological Signal Processing Algortihms for Short-Term Heart Rate and Blood Pressure Variability*. 2017.
49. ZHANG, Qiang, CHEN, Xianxiang, FANG, Zhen, XUE, Yongjiao, ZHAN, Qingyuan, YANG, Ting and XIA, Shanhong. Cuff-less blood pressure measurement using pulse arrival time and a Kalman filter. *Journal of Micromechanics and Microengineering* [online]. 1 February 2017. Vol. 27, no. 2, p. 024002. [Accessed 7 May 2019]. Available from: doi:10.1088/1361-6439/27/2/024002.
50. CHEN, W, KOBAYASHI, I T, ICHIKAWA, I S, TAKEUCHI, Y and TOGAWA, T. Continuous estimation of systolic blood pressure using the pulse arrival time and intermittent calibration. *Med. Biol. Eng. Comput* [online]. 2000. Vol. 38, p. 569–574. [Accessed 7 May 2019].
51. OGEDEGBE, Gbenga and PICKERING, Thomas. Principles and techniques of blood pressure measurement. *Cardiology clinics* [online]. November 2010. Vol. 28, no. 4, p. 571–86. [Accessed 14 May 2019]. Available from: doi:10.1016/j.ccl.2010.07.006.